AC Grid Emulations for Advanced Testing of Grid-Connected Converters - An Overview

Ma, Ke; Wang, Jiashi; Cai, Xu; Blaabjerg, Frede

Published in:
I E E E Transactions on Power Electronics

DOI (link to publication from Publisher):
10.1109/TPEL.2020.3011176

Publication date:
2021

Document Version
Publisher's PDF, also known as Version of record

AC Grid Emulations for Advanced Testing of Grid-Connected Converters—An Overview

Ke Ma, *Senior Member, IEEE*, Jiashi Wang, Xu Cai, and Frede Blaabjerg, *Fellow, IEEE*

***Abstract*—High penetration of distributed generations and active loads have enabled the power electronics converter to become a vital component in the modern power grid system, and the broad employment of grid-connected converters at various power levels is making the grid impedance and characteristics complicated. Consequently, in order to validate more advanced features such as the reliability and stability performances of the grid-connected converters, it is becoming an emerging need to emulate the grid behaviors from more aspects. This article serves to foster and investigate the state-of-the-art techniques in the field of ac grid emulation from the perspective of multiple spatial-scales and multiple time-scales. Four major concepts used for grid emulation with featured principles, including concept I (analog simulation with under-scaled components), concept II (grid characteristics in the real-time simulator), concept III (grid characteristics in the converters structure), and concept IV (grid characteristics in the converters controller), are summarized, respectively, in this article. The practical implementation regarding to the circuit topology and the power supply for the grid emulation system are also discussed. Finally, the future trends and conclusions in the field of ac grid emulation are provided.**

***Index Terms*—Grid characteristics, grid-connected converters, grid emulation, harmonic, impedance, testing.**

I. Introduction

RENEWABLE power generations, together with active loads and energy storage systems which have bi-directional power flows, have experienced tremendous development in the last two decades. Consequently, the grid-connected converters are becoming an essential component in the formation of modern power grid. Fig. 1 shows a typical construction of power electronics-intensive ac grid. In this system, sources and loads are connected to the grid ac bus through power electronics converters, which are capable of controlling the voltage/current injected into/absorb from the grid system [1]–[3]. Furthermore, when the secondary ac bus is disconnected from the primary ac bus, the power electronics converters need to act correspondingly to ensure the proper operations of the secondary ac grid.

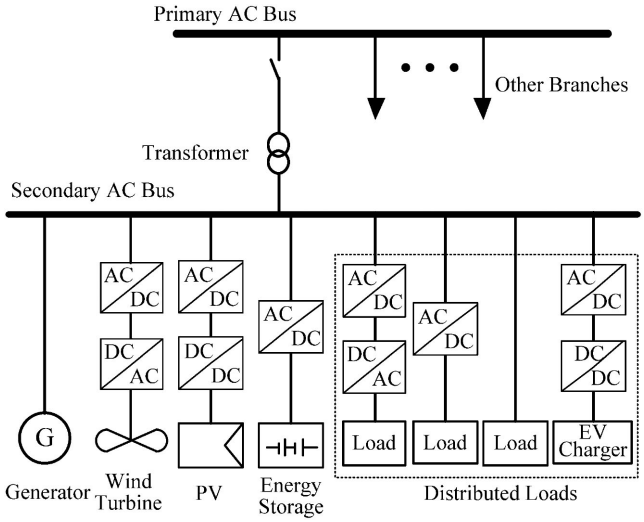

Fig. 1. Typical construction and components of modern ac power grid.

It can be seen that the grid-connected converters nowadays have more important roles to serve than they had before: not only convert the power for the generators/loads, but also participate in the regulation and operation of the power grid. Many more additional functions are supposed to be provided by the grid-connected converters, such as to maintain the grid bus voltage [4]–[6], provide power inertia [7]–[10], stabilize the grid voltage and frequency [11], [12], compensate/absorb reactive power [13]–[15], suppress the current/voltage harmonics [16], [17], ride through low/high voltage during grid faults (LVRT/HVRT) [18], [19], communicate with other grid components [20], [21], etc. Most of these features involve important contributions from the grid-connected converters, and thus imposing them with more control functions as well as more control complexities. In order to make the grid-connected converters work properly and meet the corresponding standards, it is necessary to test the grid-connected converters and validate multiple performances before connecting them to the actual grid. The potential testing items, depending on the power level and roles of the converters, should include stability [22]–[24], grid codes compatibility [25]–[28], and reliability [29]–[31]. All these features call for more advanced testing approaches, in which the grid characteristics need to be emulated more precisely from more aspects [32].

Manuscript received February 23, 2020; revised June 5, 2020; accepted July 9, 2020. Date of publication July 24, 2020; date of current version September 22, 2020. This work was supported in part by the National Nature Science Foundation of China under Grant 51777123 and in part by the Power Electronics Science and Education Development Program of Delta Group. Recommended for publication by Associate Editor G. De Donato. *(Corresponding author: Ke Ma.)*

Ke Ma, Jiashi Wang, and Xu Cai are with the Department of Electrical Engineering, Shanghai Jiao Tong University, Shanghai 200240, China (e-mail: kema@sjtu.edu.cn; jiashiwang@sjtu.edu.cn; xucai@sjtu.edu.cn).

Frede Blaabjerg is with the Department of Energy Technology, Aalborg University, 9220 Aalborg, Denmark (e-mail: fbl@et.aau.dk).

Color versions of one or more of the figures in this article are available online at https://ieeexplore.ieee.org.

Digital Object Identifier 10.1109/TPEL.2020.3011176

Basically, the power grid can be classified into ac form and dc form. The ac grid is widely employed in the transmission, distribution, and microgrid system, and it covers all the existing voltage levels in the grid network. On the other hand, the dc grid is mainly applied in the form of microgrid at low/medium voltage level [34], [35], or power transmission at medium/high voltage level [36], [37]. The major characteristics of ac grid are more complicated, including the aspects of frequency, harmonics, voltage amplitude, active/reactive power flow, and impedance. On the other hand, the major characteristics of dc grid only include the aspects of voltage amplitude, active power flow, and impedance. Although the application of dc grid has shown great potential developments in the future, the emulation of ac grid is more challenging and emerging for most of the grid-connected converters. As a result, only the technologies used for ac grid emulation is in focus in this article.

It is worth to mention that the ac grid emulation is not actually a new concept, many types of testing instrument, namely, programmable ac voltage source (PVS), have been available on the market for longer time. In the PVS-based ac grid emulator, various control schemes, such as resonant control or repetitive control [38], [39], are used to generate the fundamental and low-order harmonics of ac voltage. Besides the normal condition, the emulations of some abnormal grid voltages are also provided, such as voltage unbalance, voltage dip, or voltage surge [40], [41]. Nevertheless, these PVS-based ac grid emulators mainly focus on the emulation of steady-state voltage behaviors. The more important characteristics of modern power grid, such as multifrequency impedance and dynamics, high-order harmonics, and spatial configurations of grid components, are ignored in these PVS-based ac grid emulators.

In the past when the power electronics were not widely adopted, the power grid can be simplified as an ideal voltage source in series with a line impedance [9], [12]. However, with the higher penetration of power electronics converters, this assumption should be updated [42]. There are some emerging requirements for the emulation of the modern grid as follows:

1) With the increasing complexity of connections for distributed generations (DGs) units, loads, transmission lines, and transformers, the spatial configurations of grid components need to be reflected in the grid emulation.
2) Various grid components which compose the power grid have different control bandwidths depending on the power levels and control roles. As a result, the dynamical behaviors of the grid under different timescales or frequency ranges need to be emulated.
3) There have been more and more interactions among the grid components and the control/impedance of grid-connected converters are no longer independent, the testing for the communication and interaction among multiple converters under test (CUTs) are becoming important.

This article serves to give a comprehensive survey on the technologies used for advanced emulation of ac grid characteristics. Four concepts of emulation method, i.e., concept I—analog simulation with underscaled components, concept II—grid characteristics in the real-time simulator (RTS), concept III—grid characteristics in the converters structure, and concept IV—grid characteristics in the converters controller, are categorized, respectively. The emulated grid characteristics are summarized based on the timescales and the spatial configurations of grid components. Some important factors to benchmark the emulation performances, such as the bandwidth of reflected grid behaviors, stability of emulator, flexibility of spatial configurations, etc., are proposed and compared among different concepts. In this case, the suitable testing scenarios of each concept are discussed considering both the characteristics of emulated grids and the characteristics of emulators. The detail realizations of grid characteristics are explicated in each concept.

The rest of this article is organized as follows. Section II illustrates the classification of ac grid characteristics. The major concepts for grid emulation are described and compared in Section III. The detailed implementations and applications of concepts II–IV are explained in Section IV–VI, respectively. The circuit topology and power supply used in the ac grid emulation are discussed in Section VII. Finally, the conclusion and future trends are presented in Section VIII.

II. Classification of AC Grid Characteristics to be Emulated

In this article, the characteristics of ac grid for emulation are classified based on two aspects, i.e., the spatial configurations and the timescales of the reflected characteristics—from the perspective of grid-connected CUT.

A. Spatial Configuration

The spatial configuration of power grid is actually a complex network to be clearly defined. In this article, the grid components are categorized as power terminals and connections. The power terminals include all types of individual generator/load, or network of multiple generators/loads. The connections are defined as grid components used for power delivery/transmission, such as transformers and transmission lines. In this article, in order to distinguish the grid components that help to establish the grid behaviors, the power terminals emulated in grid emulators are defined as inputs and power terminals of CUT are defined as outputs. In this way, it is relatively easier to benchmark the complexities of grid emulators and the spatial configuration of the emulated grid. The number of outputs indicates the capability of grid emulators to test the converters. The number of inputs implies the complexity of emulated grid behaviors. In most cases, the greater number of outputs is, the more converters that the grid emulators can test; the greater number of inputs is, the more complex spatial configurations that the grid emulators can reflect. In this case, the spatial configurations of commonly seen ac grid for emulation can be categorized into single-input–single-output (SISO) type [54]–[58], multi-input–single-output (MISO) type [59]–[66], and multi-input–multi-output (MIMO) type [71]–[83].

A typical SISO-type power grid for emulation is shown in Fig. 2(a), where a generator/converter/load is considered as the input power terminals, and a grid-connected converter is considered as the CUT which is connected to the output terminal of grid emulator. If the inertia of the input power terminal is large

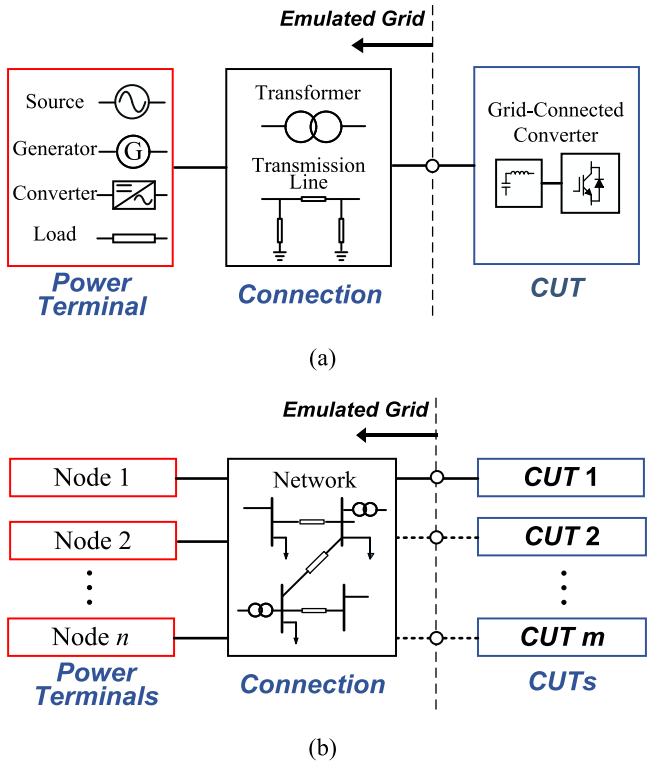

Fig. 2. Spatial configuration of grid. (a) Single-input–single-output (SISO) type grid. (b) Multi-input–single-output (MISO) type grid or multi-input–multi-output (MIMO) type grid. CUT: converter under test.

enough, it can be simplified to an ideal ac voltage source with fixed amplitude and frequency. The input and the output terminals in the grid emulation are interconnected through a "connection" part, which includes transformer and/or transmission line, as well as their geometry topology. The transformer usually appears between the medium-voltage distribution grid and the CUT, such as in the applications like wind power generation [44], [45], STATCOM, or unified power flow controller [46]. The transmission line normally appears when the scenario of "weak grid" characteristics needs to be emulated, and the line impedance will determine the short circuit ratio of the grid for emulation [33], [47].

On the other hand, Fig. 2(b) summarizes the testing scenario of typical MISO-type grid or MIMO-type grid. The multiple power terminals and CUTs are connected through a similar connection part, which in this case is a multiterminal circuit network. It may be composed of multiple transformers, sections of line impedances, and relays. The major difference between the MISO-type grid and the MIMO-type grid lies in the number of output terminals of grid emulators.

The types of emulated grid under certain spatial configuration are suitable for different testing scenarios of grid-connected converters. For example, the testing scenario of the SISO-type grid normally involves the single CUT applications with weak grid [9], [12], or the ideal grid [14]–[16]. On the other hand, the microgrid [4], [21], [28] and HVdc system [36], [37] are normally configured as the testing scenarios of MISO-/MIMO-type grid.

B. Timescales of Reflected Characteristics

The components in power grid may involve multiple bandwidths of dynamics which appear on different timescales depending on their spatial configuration. In this case, the emulated grid can be classified based on the dominant characteristics under certain timescales or frequency ranges. Some examples of grid emulations for characteristics under different timescales are provided as follows.

1) Power inertia in the emulated grid is typically provided by the synchronous generators, and can also be provided by grid-connected converters nowadays. Since the inertia of individual synchronous generator is usually larger than 10^0 kg·m^2, the bandwidth of dynamics related to the power inertia being emulated is usually below the fundamental frequency ($f_{\rm fd}$).
2) Zero-sequence and negative-sequence voltage/current typically appear in the emulation of faulty or unbalanced grid condition. In this case, the fundamental and low-order harmonics of voltage/current are the main focus to be emulated with dynamics above $f_{\rm fd}$.
3) Positive-sequence harmonics normally appear in multiple frequency ranges because of different generation mechanisms. The low-order harmonics, with frequencies below several hundreds of Hertz, are mainly excited by the nonlinear loads or the deadtime in the grid-connected converters. The medium-/ high-order harmonics are mainly caused by the switching of power semiconductor devices, with frequency ranges between several kilo Hertz to hundreds of kilo Hertz.
4) Impedance characteristics of power grid involve all frequency ranges, and they are determined by multiple factors. The passive components, such as transmission lines and filters, will determine the grid impedance under all frequency ranges. Besides, as the broad integration of power electronics, the complex control behaviors introduced by these power electronics converters, start to have nonnegligible impacts to the grid impedance under various frequency ranges. Generally, the control behaviors with relatively low control bandwidth, such as the phase locked loop, virtual synchronous generator (VSG) control, and droop control, have impacts to the grid impedance in low frequency band. On the other hand, the control behaviors with higher control bandwidth, such as the voltage control and current control, mainly have impacts to the grid impedance in high frequency band.
5) Since the impedance is reshaped in the modern power grid by the power electronics converters, the characteristics of resonance may be altered, which need to be accurately emulated under multiple frequency ranges in order to validate the stability of the interactions between the emulated grid and the grid-connected converters.

III. Concepts for AC Grid Emulation

The state-of-the-art approaches to achieve grid emulation involve four major concepts. For the sake of easier demonstration, a basic MISO-type grid for emulation is configured and

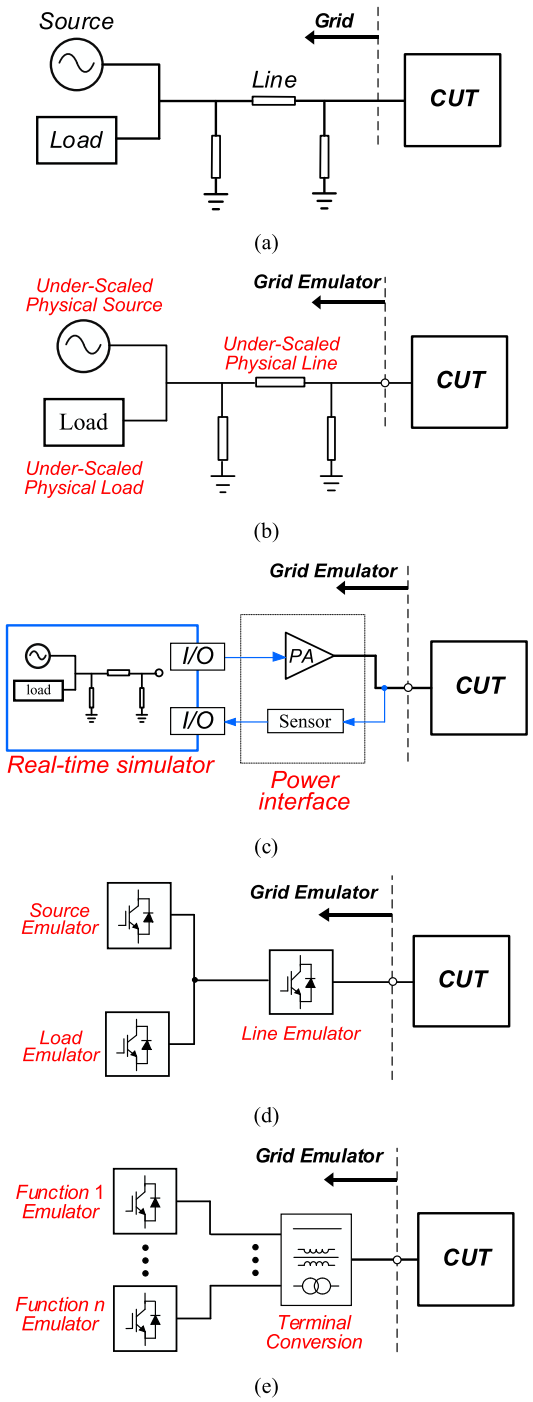

Fig. 3. Grid emulation based on three different concepts. (a) Emulated grid. (b) Grid emulator based on concept I. (c) Grid emulator based on concept II. (d) Grid emulator based on concept III. (e) Grid emulator based on concept IV. CUT: converter under test, PA: power amplifier.

shown in Fig. 3(a), which involves the most commonly seen grid components including an equivalent source, a passive load, and a section of line impedance.

In concept I, all of the components in the emulated grid are replaced with underscaled physical components, this is a common approach known as "analog simulation" in the power system analysis. The corresponding realization of grid scenario [Fig. 3(a)] by this approach is shown in Fig. 3(b). In this concept, the dynamic performances of the grid components are well retained with the mirrored spatial configuration of the targeting grid for emulation.

The concept II is also known as power hardware-in-the-loop (PHIL) from the perspective of real-time simulation. The realization of grid scenario in Fig. 3(a) based on concept II is shown in Fig. 3(c). In this concept, the characteristics of the grid components as well as their spatial configuration are implemented/reflected as simulation models in the RTS. The power amplifier, which tracks the reference voltage/current generated by RTS, is introduced to interface the CUT, and the behaviors of CUT need to be sampled by sensors and then the signals are feedback into the RTS to update the simulation model. The types of reference signals generated by the RTS for amplifier and the types of electrical signals sampled by sensors from CUT are chosen based on the adopted interface algorithm. The interface algorithms can be grouped into voltage-type and current-type. When the voltage-type algorithm is adopted, the RTS generates voltage references for amplifier and the sensors are used to sample the current in DUT. On the contrary, when the current type algorithm is adopted, the RTS generates current reference for the amplifier and the sensors sample the voltage in DUT.

The grid emulation scenario of Fig. 3(a) based on the concept III is shown in Fig. 3(d). Because of the flexible control dynamics and circuit configurations, the power electronics converters are used to emulate the electrical characteristics of grid components including generation units, loads, and line impedances. In this case, the spatial structure of the emulated grid is reflected by substituting each grid component or connection with the emulating converter employing different control functions.

The grid emulation scenario of Fig. 3(a) based on concept IV is shown in Fig. 3(e). In this concept, only the terminal characteristics of the grid seen by the CUTs are focused, and the terminal behaviors are emulated by the output behaviors of single or multiple emulating converters with corresponding control functions. In the case of multiple emulating converters, converters with different power level and control bandwidths may be designed to emulate the grid characteristics under different timescales. Due to the limits of flexibility to reflect the spatial configuration of grid components, a "terminal conversion" stage, which is composed of certain connections of transformers, coupling inductances, and/or transmission lines, may be needed in this concept to create the required testing scenarios of emulated grid.

The major differences among the four concepts for grid emulation include the bandwidth of reflected grid behaviors, stability issues, flexibility of spatial configurations, power level, cost per kilo Watt, testing efficiency, suitable testing scenarios etc., which will be discussed as follows.

A. *Bandwidth of Reflected Grid Behaviors*

The characteristics of CUTs typically lie under different frequency ranges. Hence, the bandwidth of reflected grid behaviors is a very important feature of grid emulators.

The concept I is actually an underscaled grid system with the similar behaviors but lower power, and there are no additional controllers or simulators affecting the dynamic characteristics of grid emulators. The bandwidth of reflected behaviors in concept I is determined by the underscaled physical components and the corresponding controllers. The dynamic characteristics of emulated grid and those of concept I can be seen as high consistency if accurate design of control for grid components is presented. In [49] and [50], the weak grids behaviors are emulated through voltage sources and inductance. The bandwidth of reflected grid behaviors in such cases can be seen as the same of the target grid for emulation.

The bandwidth of reflected behaviors in concept II is restrained by the time step in RTS system, as well as the control bandwidth of power amplifiers. In order to achieve the maximum bandwidth of concept II, the time step of RTS is normally configured to be small. As illustrated in [70], the time step of RTS is usually around dozens of μs [63], [72] or even a dozen ns [122]. Generally speaking, the time step configured in the RTS system is much smaller than the timescales of control dynamics in the existing power amplifiers. As a result, the bandwidth of power amplifier will determine the bandwidth of the reflected grid characteristics in the concept II.

The power amplifiers for grid emulation typically include the linear power amplifier (LPA) and the switched mode power amplifier (SMPA). The bandwidth of LPA is relatively high and is up to 50 kHz in [70]. The concept II (adopting LPA) reflects lower bandwidth of grid behaviors than concept I, but higher bandwidth than the other concepts.

On the other hand, the bandwidth of reflected behaviors in concepts II (adopting SMPA), III, and IV mainly depends on the bandwidth of emulating converters. Due to more emulating converters used in concept III, the widely used two-level converter topology is commonly adopted considering the space and cost. In this case, the bandwidth of emulating converters is limited and is usually between hundreds of Hertz and several kilo Hertz.

There are two commonly used approaches to raise the bandwidth of emulating converters in concept IV and SMPA in concept II. The first approach is adding additional high-switching-frequency circuits. In [76], two converters with different switching frequency are connected to achieve higher control bandwidth. The converter with higher switching frequency is composed of MOSFETs or SiC devices and the switching frequency can be extended above 50 kHz. The second approach is adopting topologies with higher equivalent switching frequency. For example, the power amplifier in [62] adopts six interleaved and paralleled half-bridge converters, the equivalent switching frequency is 125 kHz and the bandwidth is 5 kHz. In this case, concept IV is able to reflect higher bandwidth of grid behaviors compared to concept III.

B. Stability Issues in Grid Emulator

The stability of grid emulator itself is a very important topic, especially when considering the interaction between grid emulators and the CUTs. Apart from the stability of the grid for emulation, the stability of grid emulator is mainly determined by two factors: 1) the additional delays which are nonexistent in the emulated grid, and 2) the dynamic characteristics of power amplifiers or emulating converters in the emulator. It is noted that the delays discussed in the following parts of this article only refer to the additional delays caused by realization of grid emulation, and the delays inherently exist in the grid components for emulation are not considered.

Since there are no additional transmission delays or controllers/simulators used for grid emulation in concept I, the stability of such grid emulators only depends on the stability of the components and controls in the emulated grid.

The additional delays introduced in concept II may cause stability issues. There are four possible types of delay in concept II, i.e., the input transmission delay between RTS and sensors, the output transmission delay between RTS and power amplifiers, the computation delay caused by digital controllers, and the modulation delay caused by PWM modulation, if SMPA is employed. Without considering the dynamic characteristics of power amplifiers, the input transmission delay and output transmission delay may have stability issues which are related to the equivalent impedance of emulated grid and equivalent impedance of CUTs. The stable conditions are different while different interface algorithms are adopted, the details of such stable conditions are illustrated in [70]. In order to improve the stability of concept II, some improved interface algorithms are proposed [63], [106].

The dynamic characteristics of power amplifiers and emulating converters are influenced by many factors, such as computation delays, modulation delays, voltage/current controllers, and passive filters. Those factors make the dynamic characteristics nonideal and cause the interactions among power amplifiers and emulating converters. Such interactions may cause stability issues. The dynamic characteristics of power amplifiers and emulating converters can be depicted with state-space models or impedance models. The state-space models represent all the variables in systems and derive detailed models in time domain, the stability can be evaluated through the eigenvalue analysis, but the models are complicated to calculate and the calculation of stability evaluation is complex. The dynamic characteristics are represented in frequency domain with the impedance models and the stability can be analyzed by the electric circuit theory. The corresponding calculation of stability evaluation is easier. The details about modeling and stability analysis of converters are illustrated in [24].

C. Flexibility of Spatial Configuration of the Emulated Grid

Considering all of the components in the emulated grid need corresponding underscaled physical replacements in concept I, the change of grid behaviors normally involves the modification of hardware. Such disadvantage limits the typical orders of magnitude on components (OMC) in concept I and makes it become expensive and difficult to vary and expend the spatial configuration of the grid for emulation. A dynamic simulation system with two generators is proposed for the test of resonance fault current limiter in [51]. In [52], a power system simulator composed of four generators and loads are proposed for the test

of static reactive power compensator. In these cases, the OMC is around 10 which is hard to be increased.

The models of the emulated grids are built and real-time simulated in the RTS system when concept II is adopted, thereby it is relatively easy to reflect various spatial configurations of grid components in the emulated grid. Considering the computing power of RTS, the typical OMC in concept II can be up to 100. In [61], some cases of simple power system, such as two paralleled synchronous generators, a transformer with on load tap charger, and low voltage distribution network, are emulated in RTS. The "Benchmark System for Network Integration of Renewable and Distributed Energy Resources" is emulated through concept II in [65]. In [67], the IEEE 123 and 8500 nodes test system are emulated in the proposed off-the-shelf non-PHIL software tools. In this case, the flexibility of grid reconfiguration in concept II is much higher.

With respect to the concept III, the number of emulating converters is mirrored to the number of grid components in the emulated grid. As a result, the spatial configuration of grid components is also difficult and expensive to be expanded. Considering the limitations of cost and space, the OMC of concept III is normally restrained to 10. In [96], a grid emulator is built with four generator emulators, two load emulators, and one long-distance transmission line emulator to emulate a two-area power system. An underscaled four-terminal HVdc system is emulated through four two-level converters in [97]. It is seen that the reflected spatial configurations in concept III represent slightly higher flexibility compared with concept I, but lower flexibility compared with concepts II and IV.

With respect to the concept IV, the model of emulated grid is real-time simulated in the controller of emulating converters, which means concept IV presents higher flexibility of spatial configuration than concepts I and IV. Due to the limits of the computing power for digital controller, the typical OMC emulated in concept IV is about 10. A modified IEEE 13 buses system is emulated through a three-phase four-leg converter in [98]. The spatial configuration of grid components is not so flexible to be reflected in concept IV compared with concept II.

D. Power Level, Testing Efficiency, and Cost

The capability of testing power for CUTs in concept I is the lowest among the four concepts considering the limitation of underscaled physical components. The reported power level at the output port of grid emulator is 700 V·A in [52] and 2.5 kV·A in [53].

Considering the relatively lower conversion efficiency of LPA, the power level of concept II (adopting LPA) is typically low and is reported at 1.2 kV·A in [75]. Generally, the testing power of concept II (adopting LPA) is lower than those of concepts II (adopting SMPA), III, and IV. The topologies of emulating converters in concept II usually adopt simple topologies, such as two-level converter [94], [97]. However, the topologies of concepts III and IV (adopting SMPA) can adopt multilevel converter, such as modular multiphase multilevel converter [56] and NPC [115], with less constraint of space about converters. The power level of concept II (adopting SMPA) is reported at 200 kV·A in [62] and 7 mil V·A in [115]. The power level of concept IV is achieved at 1 mil V·A in [93].

The overall efficiency of concept I depends on the passive elements in the grid emulators, and the overall testing efficiency of concepts II (adopting SMPA), III, and IV is determined by the number, topology, and switching frequency of the emulating converters in the grid emulator. Thus, it is hard to compare the testing efficiency of the four concepts. But generally speaking, the testing efficiency of concept I and concept II (adopting LPA) are the lowest on the similar emulation capability due to the large number of passive elements in concept I and the low testing efficiency of LPA [107].

With respect to the cost, the system based on concept I is much expensive owing to expensive physical elements, such as generators and transformers. And such physical elements are more expensive than converters in most cases. Therefore, the cost of per Watt in concept I is higher than that in concept III and concept IV. The concept II is normally more expensive than the other concepts because of the RTS, therefore it is only suitable to be used in the emulation scenario of complex grid network with lots of grid components. And the concept II (adopting LPA) is usually more expensive than concept II (adopting SMPA) at the similar capability because of the higher cost for LPA. The cost of concept III depends on the spatial configuration of the emulated grid. With the increasing number of grid components to be emulated, the cost of concept III will increase. The number of converters in grid emulators determines the cost of concept IV. Considering the usual number of converters is 1 [79], [80] or 2 [89], the cost of concept IV is usually lower than other concepts.

E. Suitable Testing Scenarios

The concept I is usually applied for dynamic simulation and analysis of power system. Some typical control functions, such as fault location method [48], fault current limiter [51], reactive power compensation [52], are tested through concept I. Owing to emulation of broad and realistic frequency ranges of grid behaviors, concept I is suitable for the stability test of grid-connected converters. In [49] and [50], the weak grid composed of ideal voltage sources and inductance is emulated with physical components to test the converter stability. However, due to the limited flexibility to reconfigure the grid for emulation, the testing functions in microgrid and system with complex control methods are rarely reported through concept I.

Considering the highest flexibility of spatial configuration, the concept II is more suitable to emulate the power grid with complex spatial configurations. Thus, the more complex control functions of grid-connected converters can be tested in concept II. The islanding detection is tested in [72] and switch from grid-connected to off-grid of microgrid is tested in [61]. Although the bandwidth of reflected behaviors is relatively high in concept II, the concept II is barely used for stability test due to the stability issues caused by the input transmission delay and output transmission delay by employing RTS. The inherent stability

issues related to the interface algorithms make it difficult to reproduce the instability phenomenon.

Because the interactions among different converters are relatively easy to be achieved in concept III, the concept III is very suitable to reflect the characteristics in MISO-type grid or MIMO-type grid. The cooperation among different converters, such as cooperation control, communication, and protection, are easy to be test in concept III. The communication and different control schemes of HVdc are tested in [97]. Nevertheless, the spatial-scales and timescales of the emulated grid are strictly limited by the control bandwidth of the emulating converters, thus the stability tests and complex control function in microgrid are hard to be conducted by concept III.

Considering the higher bandwidth and the fewer types of additional delays, the concept IV is able to reflect the grid characteristics within wider frequency ranges. This feature makes concept IV a suitable approach for stability test of grid-connected converters. On the other hand, the flexibility of spatial configuration is easy to achieve within the limited OMC, and the control function in small-scaled microgrid is easy to be tested. The operation in a modified IEEE 13 bus system is tested in [98].

F. Comparison and Categorization of Different Concepts

The comparisons of abovementioned capabilities among the three concepts for grid emulation are summarized in Table I.

There are no additional components and controllers/simulators in concept I, the emulated dynamic characteristics under different timescales are reflected in same way. Hence, the concept I cannot be categorized based on the timescales and the categorization of concept I is not illustrated in Fig. 5. The approaches of other three concepts for grid emulation can be categorized from the perspective of multiple spatial-scales and multiple timescales. The categories based on spatial-scales of the three concepts are the same, i.e., all the three approaches can be classified into SISO-type, MISO-type, and MIMO-type.

On the other hand, the timescales-based categories of the three concepts are not completely the same and will be discussed as follows: Based on the implementations of control system in different concepts, the timescales are divided into control reference level, controller level, modulation level, and circuit level. Considering the relatively high control bandwidth of emulating converters or power amplifiers introduced in the emulators, the grid characteristics under fundamental frequency (f_{fd}), i.e., under control reference level, can be emulated through adjusting the control references of voltage/current control loop. The grid characteristics between f_{fd} and the bandwidth of voltage/current controller in the emulators can be emulated through designing the used controller, and these frequency ranges of emulation are named as controller level. The emulation is realized by modifying the modulation signals in modulation level, whose frequency ranges lie between the bandwidth of voltage/current controller and the switching frequency of the converter.

Additional high-bandwidth converter with higher switching frequency but lower power level is needed in circuit level, which is responsible for emulating the grid characteristics above switching frequency.

Based on the classifications of ac grid characteristics under different timescales and spatial-scales, the relevant literatures on different concepts for grid emulation can be categorized, as illustrated in Fig. 4. In the following, the detail implementations and features for the three concepts of grid emulation, will be reviewed and discussed.

IV. AC Grid Emulation Based on Concept II

In this concept, the RTS and the CUT are connected through a power interface. The control of the power interface is chosen based on the adopted interface algorithm. There are three common kinds of interface algorithms reported in both voltage-type algorithm and current-type algorithm, i.e., ideal transformer model (ITM), partial circuit duplication (PCD) and damping impedance method (DIM). The comparisons among the three interface algorithms are illustrated in [70], [106]. The interface algorithm will determine the control methods for power amplifiers in the power interface. Taking the voltage-type ITM as an example, the configuration of concept II is demonstrated in Fig. 5(a), where the RTS sends voltage references to the power amplifier. And the power amplifier adopts a current controller when the interface algorithm is current-type. The corresponding configuration is shown in Fig. 5(b).

There are three types of power amplifiers reported in the field of grid emulation, i.e., SMPA [56], [63], generator-type amplifier [59], and LPA [72]. The bandwidth of LPA and SMPA are up to dozens of kilo Hertz, while the bandwidth of generator-type power amplifier is much lower because of the larger inertia in the used generator. The power level of generator-type power amplifier is less than that of SMPA because of the constraint of testing space. In this case, the generator-type power amplifier has limited advantages over bandwidth and power level compared with LPA and SMPA, as a result, LPA and SMPA are usually adopted in concept II. The concept II (adopting generator-type power amplifier), therefore, is not detailed in this article. The details of LPA and SMPA are illustrated in Section VII.

When different types of power amplifiers are adopted, the corresponding control methods are employed. The typical single-phase implementation for LPA-based grid emulator is shown in Fig. 6, and the three-phase implementation is similar except for the number of phases. The LPA receives the voltage reference (v^*) from RTS, and the voltage controller generates the drive signal (e) for the amplifier. Thanks to the fast response time to the control references, the linear amplifier can employ analog circuit-based controller to further enhance the control dynamics without time delays. On the other hand, the digital controller is easier and more robust to be realized, but there are multiple time delays in the digital control loops [106], [107].

The LPA has much lower efficiency and higher power loss during power conversion; as a result, the power level and testing efficiency for the grid emulation are seriously limited with the high cost per Watt. The configuration of SMPA-based concept II and LPA-based concept II are similar. The differences lie in

TABLE I
COMPARISONS OF DIFFERENT CONCEPTS FOR GRID EMULATION

Characteristics \ Concept		Concept Ⅰ: Analog simulation with under-scaled components	Concept Ⅱ: Grid characteristics in real-time simulator by adopting LPA	Concept Ⅱ: Grid characteristics in real-time simulator by adopting SMPA	Concept Ⅲ: Grid characteristics in converters structure	Concept Ⅳ: Grid characteristics in converters controller
Bandwidth of reflected grid behaviors	**Limits**	No limits	Discrete time of RTS, bandwidth of LPA	Discrete time of RTS, bandwidth of SMPA	Bandwidth of converters in grid emulator	Bandwidth of converters in grid emulator
	Ranking	Highest	Higher	Medium	Low	Medium
	Typical number	up to infinite[49,50]	50 kHz [70]	5 kHz [62]	up to several kHz [96,97]	3.2 kHz [12]
Types of additional delay in realization		No	Input transmission delay in RTS, output transmission delay in RTS, computation delay	Input transmission delay in RTS, output delay transmission in RTS, modulation delay, computation delay	Modulation delay, computation delay	Modulation delay, computation delay
Stability-related issues		No	Interface algorithms; dynamic characteristics of LPA	Interface algorithms; dynamic characteristics of SMPA	Dynamic characteristics of converters in grid emulator	Dynamic characteristics of converters in grid emulator
Spatial configurations	**Achievement of spatial configuration**	Replacing each emulated component with physical component	Real-time running the model of emulated grid in RTS		Replacing each emulated component with converter	Real-time running the model of emulated grid in controllers of converters
	Flexibility to reconfigure	Hardest	Easy		Harder	Medium
	Typical number of emulated components	Less than 10 [51, 52]	More than 100 [65,67]		About 10 [96]	About 10 [98]
Power level	**Ranking**	Low	Low	High	Medium	High
	Typical number	700 VA [52], 2.5 kVA [53]	1.2 kVA [75]	200 kVA [62], 7 MVA [115]	15 kVA [96]	1 MVA [93]
Efficiency	**Efficiency-related issues**	Passive components in grid emulators	Power efficiency of LPA	Power efficiency of SMPA	Power efficiency of converters in grid emulator	Power efficiency of converters in grid emulator
	Ranking	Low	Medium	High	High	High
Cost per Watt	**Most costly components**	Physical components in grid emulators	RTS, LPA	RTS, SMPA	Converters in grid emulators	Converters in grid emulators
	Ranking	Medium	Highest	Higher	Lower	Lowest
Typical testing functions		Stability [49, 50], control in power system [48, 51, 52]	Operation in microgrid [61, 67], complex control functions [72]		Cooperation among different converters (communication, protection, control) [96, 97]	Stability, operation in small-scaled microgrid [98]

LPA: Linear power amplifiers; SMPA: switching-mode power amplifier; RTS: real-time simulator.

Concept II
Concept III
Concept IV

Reference Frequency &Characteristics / Spatial Structure		*SISO*	*MISO/MIMO*
Reference Level	Inertia, Impedance, Fault condition, Fundamental steady state	[54-58] [77-90] [38,39,77-93]	[59-75] [94,96,97] [98]
Control Level	Low/Medium frequency impedance, Low/Medium frequency harmonics	[40,61] [89,99] [38,39,89-95]	[74] [97] NF
Modulation Level	Medium frequency impedance, Medium frequency harmonics	 NF [100-103]	 NF NF
Hardware Level	High frequency impedance, High frequency harmonics	[76] [11,12,91,104]	NF NF

Fig. 4. Classification of recent research on grid emulation based on spatial configuration and frequency ranges. SISO: single-input-single-output, MISO: multiple-input–single-output, MIMO: multiple-input–multiple-output, NF: not found.

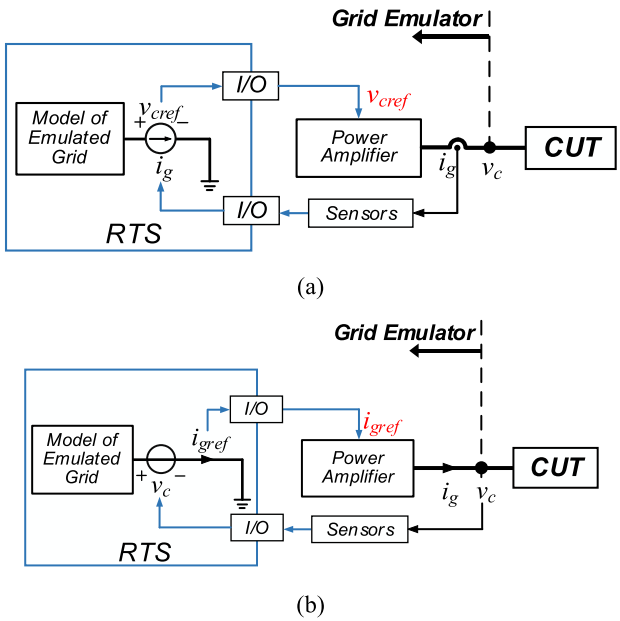

Fig. 5. Grid emulation based on concept II. (a) Adopting voltage-control algorithm. (b) Adopting current-control algorithm. RTS: real-time simulator, CUT: converter under test.

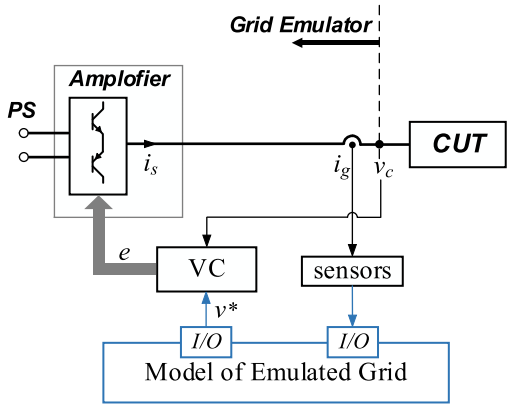

Fig. 6. Power amplifier based on linear power amplifier. PS: power supply, VC: voltage controller, RTS: real-time simulator, CUT: converter under test.

the control methods and the control bandwidth. More complex control methods, like repetitive controller (RC) [40], and linear quadratic optimal regulator [123], can be adopted in SMPA.

V. AC Grid Emulation Based on Concept III

In this concept, the components in the emulated grid are replaced by power electronics converters with different control functions and circuits. Typically, the power terminals are replaced by dc/ac converters and the connections are replaced by two back-to-back connected dc/ac converters. The power terminals in the emulated grid can be classified into the voltage source and the current source. The voltage sources normally refer to the grid components which participate in the forming of the grid bus voltage, including generators and DGs which participate in

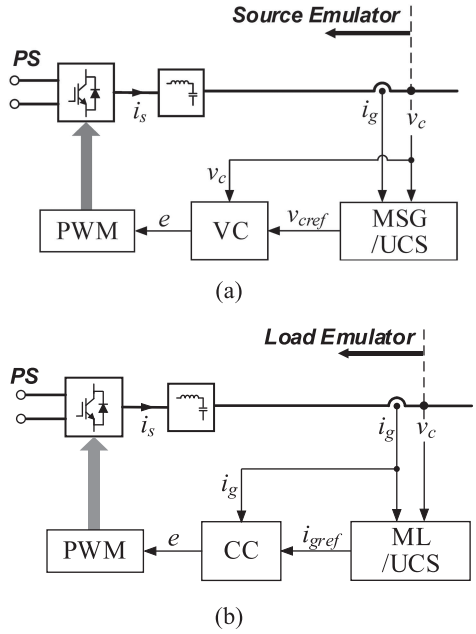

Fig. 7. Control method of power terminal emulator. (a) Typical-source emulation. (b) Typical load emulation. PS: power supply, VC: voltage controller, CC: current controller, MSG: model of synchronous generator, UCS: upper control system, ML: model of load.

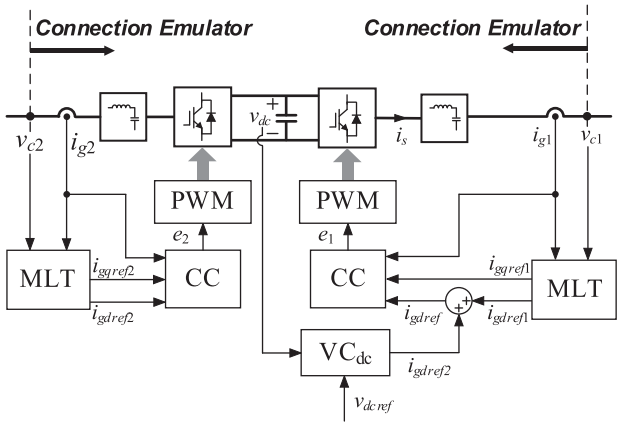

Fig. 8. Typical control method of connection emulator with dc voltage control. VC: voltage controller, CC: current controller, MLT: model of line or transformer.

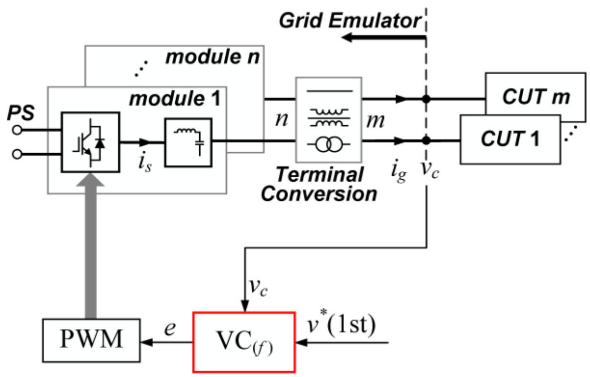

Fig. 9. Steady-state emulation at the control reference level. PS: power supply, VC: voltage controller, CUT: converter under test.

the grid manipulation. The behaviors of these sources can be emulated by using the voltage-controlled converter as shown in Fig. 7(a), the model of synchronous generator or upper control system generates the fundamental voltage references and then sends them to the voltage controller [78], [97]. On the other hand, the current sources in the emulated grid mainly refer to the loads, DGs without grid-forming functions, ESS, STACOM, and APF. The behaviors of these current sources can be emulated by using a current-controlled converter as shown in Fig. 7(b), the model of load generates the required current references and then sends them to the current controller [94].

The back-to-back converters used for the emulation of grid connections are shown in Fig. 8. The control loops of two converters are similar with same model of lines or transformers except for the additional dc voltage controller in one of the converters. The dc bus controller generates another current reference i_{gdref2}, and the current reference in d-axis i_{gdref} is the sum of i_{gdref1} and i_{gdref2}. The controllers under different frequency ranges will be illustrated in Section VI.

VI. AC Grid Emulation Based on Concept IV

In the concept of grid emulation based on concept IV, the emulation of grid is achieved though the models built in controllers of emulating converters. The emulation characteristics under different frequency ranges involve different control methods and different bandwidths. The characteristics of grid for emulation under different timescales are achieved by different levels of control in the emulating converters, i.e., control reference level, controller level, modulation level, and circuit level.

A. Emulation Under Control Reference Level

The control structure and power stage used for emulation of steady-state grid behaviors below fundamental frequency are illustrated in Fig. 9. The power stage in this case is composed of n emulating modules, a terminal conversion part, and m CUTs. An emulating module indicates a single-phase emulating converter, including power semiconductors and filters. The "terminal conversion" part transfers the output of n emulating modules into an m-line system, which can match with the required line conditions of CUTs.

The voltage controller $\mathrm{VC}_{(f)}$, shown in Fig. 9, is able to track the voltage reference v^*(first) at fundamental frequency. Such voltage reference values are coming from the given grid specifications or behaviors, which are not affected by the CUTs. This reference values can also include harmonics and the corresponding control configurations are illustrated in the latter sections. Those designs are consistent with most of the grid integration applications and will ensure simplicity and stability during the test. The control loop can adopt double-loop voltage control method or other advanced control strategies, for example, repetitive control [38], [39].

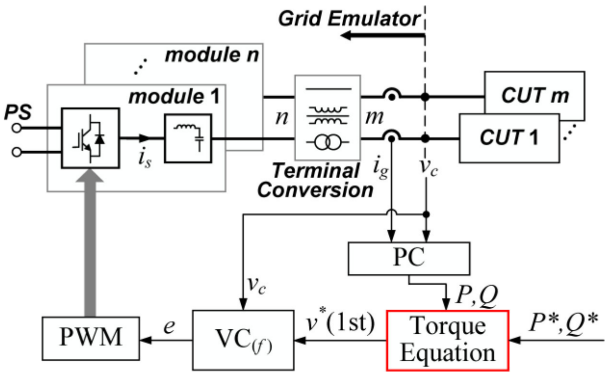

Fig. 10. Emulation of inertia. PS: power supply, VC: voltage controller, PC: power calculation, CUT: converter under test.

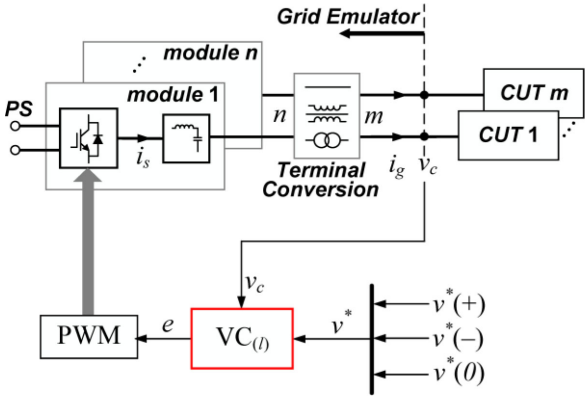

Fig. 11. Fault emulation. PS: power supply, VC: voltage controller, CUT: converter under test.

The models of synchronous generators are very complex because of the complex magnetic circuit model, to simplify the analysis, only the inertia reflected by swing equation is considered here. The emulation of power inertia in the concept IV can be achieved by adopting the VSG control mode in the emulating converters. The configuration of VSG for grid emulation is shown in Fig. 10, which is achieved in the torque equation programed in the controller. Since the time constant of emulated inertia is much larger than the time constant of voltage control loop, the voltage control loop can be considered as an ideal transparent link in this case. The modeling and parameters design of VSG have been described in [85] without considering the dynamical characteristics of the voltage control loop. The work in [81] illustrates the power response capability between droop control and VSG control when assuming the output voltage is able to track the given voltage reference from torque equations ideally.

The configuration of grid fault emulation based on concept IV is illustrated in Fig. 11. When the number of m is 3 or 4, the CUT is three-phase-three-line system or three-phase-four-line system, and the corresponding emulated grid is three-phase grid. The faults in such three-phase grid include asymmetric faults and symmetric faults. The grid voltage under asymmetric fault contains components under different sequence. As a result, v^* may include positive-sequence voltage reference $v^*(+)$, negative-sequence voltage reference $v^*(-)$, and zero-sequence voltage reference $v^*(0)$ [41], [88].

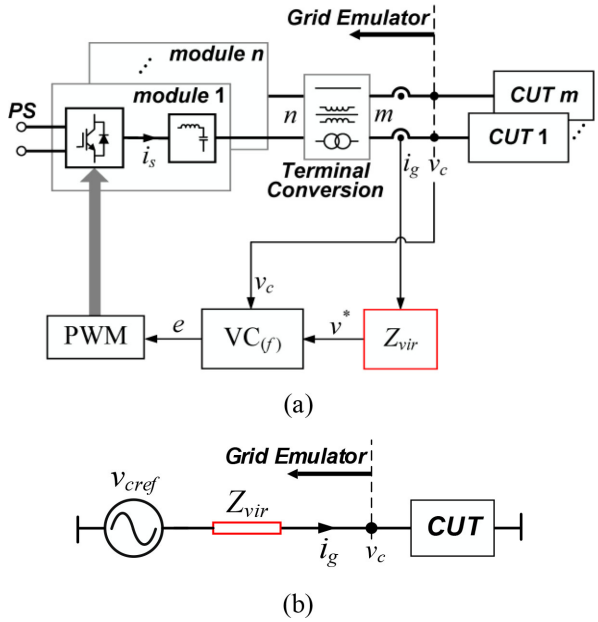

Fig. 12. Virtual impedance at the control reference level. (a) Configuration of virtual impedance. (b) Equivalent circuit of virtual impedance. PS: power supply, VC: voltage controller, CUT: converter under test.

The configuration of virtual impedance at the control reference level is shown in Fig. 12(a). The voltage reference with virtual impedance (v^*) is

$$v^* = v_{\text{cref}} - i_g Z_{\text{vir}}. \tag{1}$$

Assuming the output voltage v_c can track the given reference v^* ideally without gain distortion, the v^* in (3) is replaced by v_c, and the new equation is

$$v_c = v_{\text{cref}} - i_g Z_{\text{vir}}. \tag{2}$$

The equivalent circuit of (3) is shown in Fig. 12(b), the virtual impedance Z_{vir} is series connected to v_{cref}. The virtual impedance at the control reference level is usually used for adjusting reactive power sharing among different droop-controlled converters since the reactive power sharing is affected by the output impedance of converters at the fundamental frequency [90]. An adjustable virtual impedance is proposed in [110] to adjust the dynamic characteristics of power control loop.

B. Emulation Under Controller Level

Fig. 13 shows the configuration of steady-state emulation of grid characteristics at the controller level. The voltage reference v^* includes the fundamental reference v^*(first) and low-order harmonics reference, namely the lth order reference $v^*(l\text{th})$ whose frequency ranges are usually around hundreds of Hertz. The voltage controller, VC$_{(l)}$, is able to achieve error-free tracking of fundamental and low-order harmonic references. Proportional multiresonant controller or RC [38], [39] are normally adopted as the used VC$_{(l)}$.

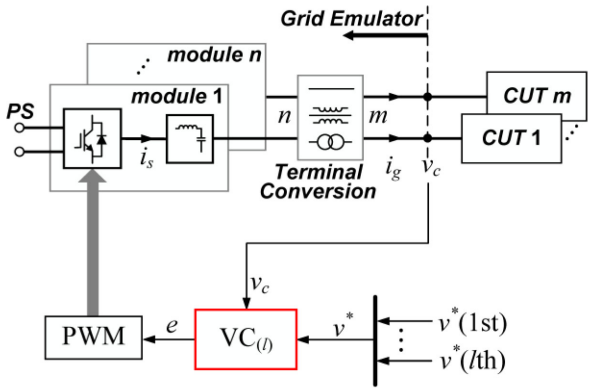

Fig. 13. Steady-state emulation at the controller level. PS: power supply, VC: voltage controller, CUT: converter under test.

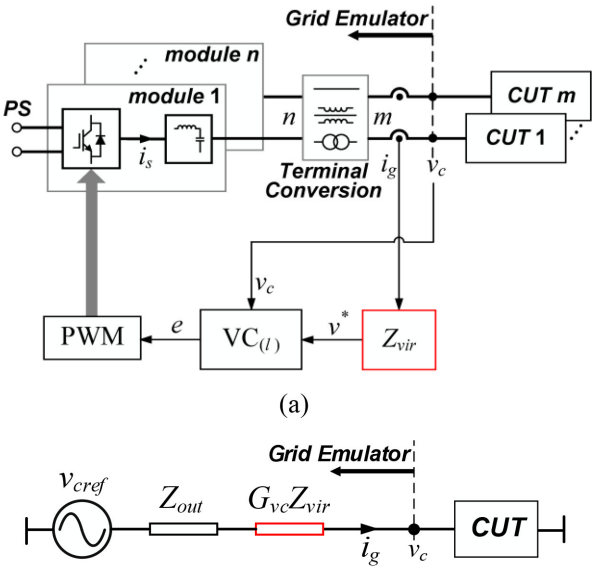

Fig. 14. Virtual impedance at the controller level. (a) Configuration of virtual impedance. (b) Equivalent circuit of virtual impedance. PS: power supply, VC: voltage controller, CUT: converter under test.

The impedance emulation under controller level is shown in Fig. 14(a). In the case of emulating the grid impedance in controller level, the dynamic behaviors of the voltage control loop in emulating converters need to be considered. The model of the voltage-controlled converter is represented as

$$v_c = G_{vc}v^* - Z_{\text{out}}i_g \tag{3}$$

where G_{vc} is the closed-loop transfer function of voltage loop and Z_{out} is the output impedance of converter.

By combining (2) and (4), the model of emulating converters with virtual impedance at the controller level is represented as

$$v_c = G_{vc}v_{\text{cref}} - G_{vc}Z_{vir}i_g - Z_{\text{out}}i_g. \tag{4}$$

The equivalent circuit for the grid emulation is shown in Fig. 14(b), and the equivalent virtual impedance is $G_{\text{vc}}Z_{\text{vir}}$. The

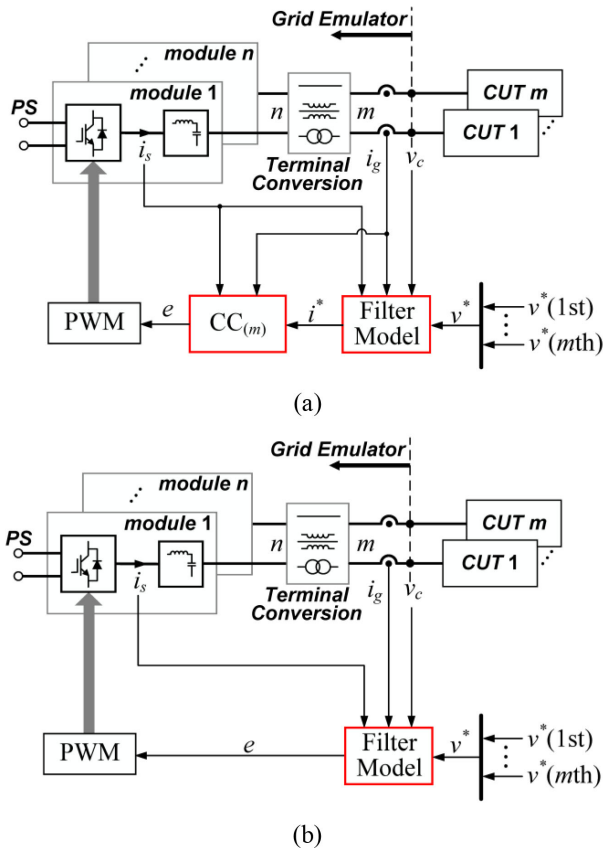

Fig. 15. Steady-state emulation at the modulation level. (a) Indirect voltage control based on current control. (b) Indirect voltage control based on modulation. PS: power supply, CC: current controller, CUT: converter under test.

virtual impedance proposed in [90], [95] is designed to suppress the low-order harmonics.

C. Emulation Under Modulation Level

Fig. 15 shows the configuration in the emulation of steady-state grid characteristics at the modulation level. Because the frequency range of emulated harmonics, i.e., $v^*(m\text{th})$, is usually around several kilo Hertz, and may be over the control bandwidth of the voltage control loop in emulating converter, the closed-loop voltage control method in this case probably is unable to track given control reference. Indirect voltage control method, therefore, is adopted to track the medium-order harmonic voltage references. Since the bandwidth of current control loop or Nyquist frequency of the modulation is larger than the bandwidth of voltage control loop, the voltage control reference is first transformed into the current control reference (i^*) or the modulation signal (e) according to the vector relationship among voltage, current, and modulation signals. The configurations of the grid emulation are shown in Fig. 15(a) and (b), respectively. Indirect voltage control of LC converter is shown in [103] and the grid-side current of LCL converter is regulated by controlling the capacitive voltage in [105].

The virtual impedance emulation achieved in the modulation level of emulating converter is shown in Fig. 16(a). In this case, the virtual impedance is achieved by adjusting the modulation

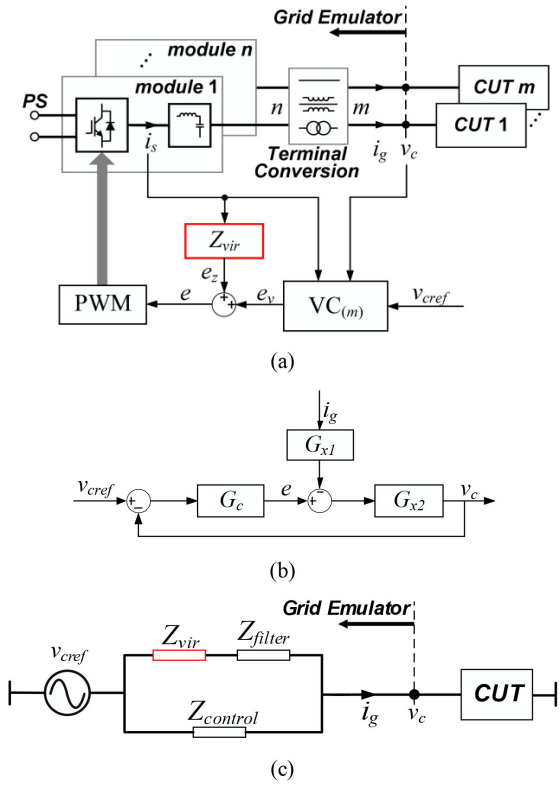

Fig. 16. Virtual impedance at the modulation level. (a) Configuration of virtual impedance. (b) Control circuit of system. (c) Equivalent circuit of virtual impedance. PS: power supply, VC: voltage controller, CUT: converter under test.

signals. The output impedance of the converter is determined by the control method and the parameters of filters. Since the virtual impedance is placed between the filter and the semiconductors, the virtual impedance is considered as a part of the filter. The equivalent circuit of the converter without virtual impedance is shown in Fig. 16(b). G_c is the transfer function of voltage controller, G_{x1} indicates the transfer function between output voltage and modulation signal, $-G_{x1}{\cdot}G_{x2}$ is equal to the impedance of the filter (Z_{filter}). The output impedance Z_{out} is

$$Z_{\text{out}} = -\frac{i_g}{v_c} = -G_{x1}\cdot\frac{G_{x2}}{1+G_{x2}G_c} = -G_{x1}\cdot\frac{1}{1/G_{x2}+G_c}$$
$$= -G_{x1}G_{x2}\frac{1}{G_c}\frac{G_c/G_{x2}}{1/G_{x2}+G_c}. \quad (5)$$

The Z_{out} can be considered as two parallel impedances, one equals to Z_{filter}, and the other equals to $-G_{x1}/G_c$. Thus, the virtual impedance is placed in series with Z_{-}. Defining G_{x1}/G_c as Z_{control}, then the equivalent circuit is shown in Fig. 16(c). The virtual impedance achieved by adjusting the modulation signals is proposed in [100]–[102] to adjust the harmonics of the output voltage and current.

D. Emulation Under Circuit Level

According to the Shannon sampling theorem, the digital control method is incapable of controlling the variables whose frequency range is beyond the Nyquist frequency. In order to track the high-frequency harmonics in voltage control reference, $v^*(n\text{th})$ (whose frequency is usually around several or dozens of kilo Hertz), another independent control method with higher sampling frequency and higher control bandwidth is adopted. The configuration of the system is shown in Fig. 17 and there are two independent control loops. The low-frequency control loop (LFCL), including the voltage controller $\text{VC}_{(l)}$ and the modulator PWM_l, is introduced to control the fundamental and low-order given voltage references. The high-frequency control loop (HFCL) is composed of voltage controller $\text{VC}_{(h)}$ and modulator PWM_h and is responsible for tracking the high-order voltage references. Considering the aliasing caused by multi-sampling, the switching frequency needs to be even higher, which means the switching frequency of PWM_h is usually higher than that of PWM_l. The modulation signals, i.e., m_l and m_h are sent into different emulating modules. Two converters with different sampling frequencies are connected in parallel [91] to track the high-frequency harmonics in the grid voltage.

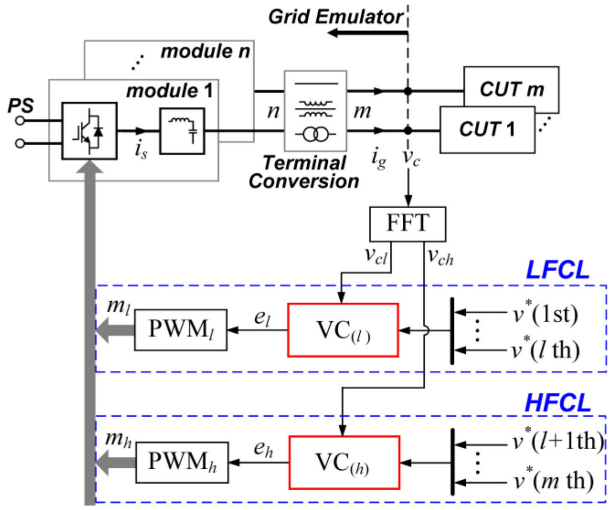

Fig. 17. Steady-state emulation at the circuit level. PS: power supply, VC: voltage controller, CUT: converter under test, LFCL: low-frequency control loop, HFCL: high-frequency control loop.

The configuration of virtual impedance in the grid emulation under the circuit level is shown in Fig. 18(a), in this case, a current control loop with higher control bandwidth and higher sampling frequency is added. Assuming the emulating modules controlled by two independent control loops are connected in series, the equivalent circuit is shown in Fig. 18(b). On the contrary, the equivalent circuit connected in parallel is shown in Fig. 18(c). A parallel-connected virtual impedance is proposed in [11], [12] to improve the stability of the emulating system.

VII. Circuit Configuration and Power Supply

A. Circuit Configuration of Concepts III and IV, and Power Amplifier in Concept II

The circuit configurations of concepts IV, III, and II are classified by three different aspects, i.e., the number of phases, type of circuit, and emulating modules.

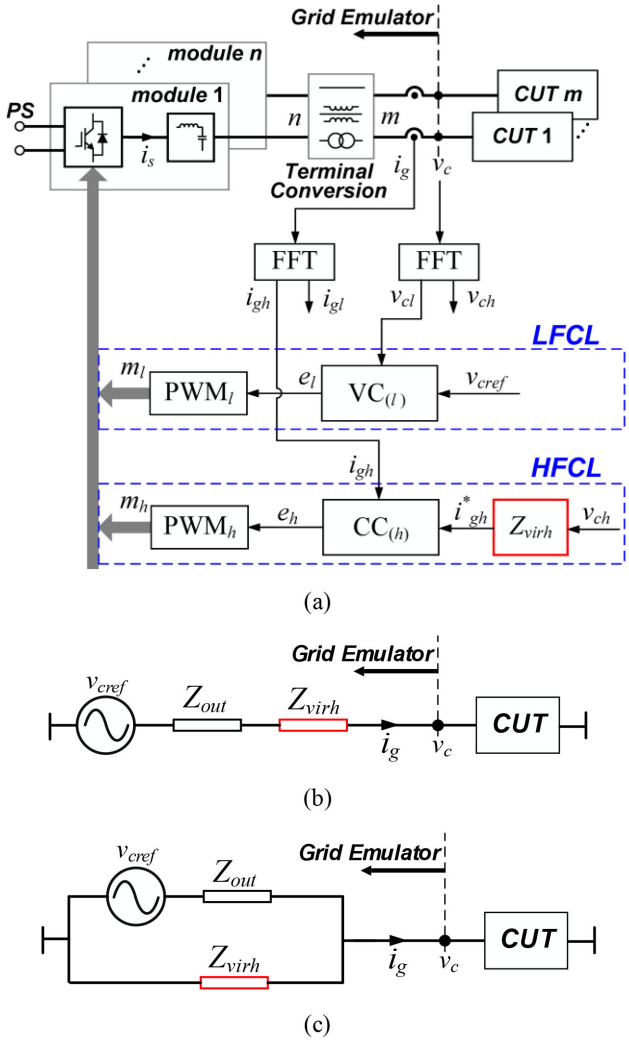

Fig. 18. Virtual impedance at the circuit level. (a) Configuration of virtual impedance. (b) Equivalent circuit with series connection. (c) Equivalent circuit with parallel connection. PS: Power supply, VC: voltage controller, CC: current controller; CUT: converter under test, LFCL: low-frequency control loop, HFCL: high-frequency control loop.

Based on the number of phases, the circuit configurations are classified into single-phase and multiphase. The main difference of these two kinds of systems is the flexibility to archive the required harmonic components for emulation. In the single-phase systems, it is relatively easy to generate the required orders of harmonics, while there are some limitations for the possible harmonic components in multiphase systems due to the lack of zero-sequence and certain orders of harmonics. In this case, in order to emulate the arbitrary voltage/current behaviors, some special circuits, such as three-phase four-leg converter [98], or three-phase full-bridge converter, are adopted for easier grid emulation.

The circuit configurations can be classified into linear-type circuits, switching-type circuits, and hybrid circuits. The linear-type circuits are based on linear amplifiers using BJT and MOSFET [113], [114]. Unlike the power semiconductors operated in switching mode, the semiconductors in linear type circuits work in amplified mode. The commonly seen linear-type circuits include class-A power amplifier, class-B power amplifier, and class-AB power amplifier [116].

The switching-type circuits are mainly based on dc–ac power electronics converters. The topologies of dc–ac converters are chosen based on the power scale and frequency range of the grid behaviors to emulate. Modular multiphase multilevel converter is adopted in the solution of [56], and four paralleled NPC converters are selected in [115]. In order to control the voltage or current under different frequency ranges, several converters which are connected in series or in parallel with different switching frequencies/power levels are adopted in [10], [11], [76].

In addition to the switching-type circuits and linear-type circuits, there are hybrid circuits reported in the field of grid emulation [107], [114]–[116]. In this solution, the switching-type converter generates or absorbs most of the power required by CUTs, and the linear-type converter is responsible of reshaping the output voltage waveforms of the emulator [107]. Based on connections of switching-type converter and linear-type converter, the hybrid circuits for grid emulation can be classified into three kinds, i.e., envelope configuration, series configuration, and parallel configuration [107].

The linear-type circuit is capable of amplifying the input signals with little distortion and high bandwidth. However, working in the amplified area leads to larger power loss and lower conversion efficiency in the circuits. The low efficiency constrains the power scale of linear-type circuit. The switching-type type circuit has higher conversion efficiency because the semiconductors work in switching mode. But working in switching mode introduces the voltage/current ripples at the switching frequency, and the output waveform is distorted. In order to filter the switching harmonics, passive filters have to be employed in switching-type circuits, and the passive filters limit the control bandwidth of switching-type circuits and increase the cost.

The circuit configuration can be classified into centralized-control system and distributed-control system. All the emulating modules are controlled by the same control loop in the centralized-control system, while there are multiple control loops for each emulating module introduced in the distributed-control system. The emulating module can be in the form of linear-mode power amplifiers or switch-mode power electronics converters, and all the emulating modules are connected through a "terminal conversion" part. Emulating modules in the distributed-control system is designed to achieve different control functions. In [76], two converters with different control bandwidths are connected in series to track the control references under different frequency ranges. In [110], a voltage-controlled converter and a current-controlled converter are connected in parallel, and the voltage-controlled converter is responsible for maintaining the output voltage of grid emulator, and the current-controlled converter is designed to share the power load with the voltage-controlled converter.

By considering the number of phases, the grid emulation with centralized control can be further classified into single-phase system and three-phase system. The configurations of terminal conversion part are different in these cases. In single-phase emulating system, the emulating modules are connected in series or in parallel without additional passive connections, as shown

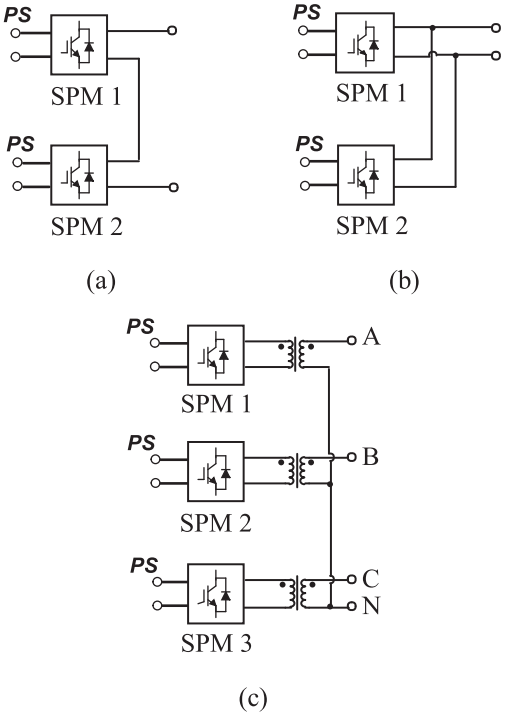

Fig. 19. Multimodule systems based on single-phase modules. (a) Series-connected system. (b) Parallel-connected system. (c) Three-phase system based on three individual SPMs. PS: power supply, SPM: single-phase module.

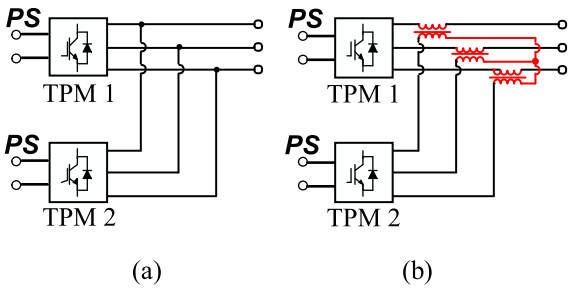

Fig. 20. Multimodule systems based on three-phase modules. (a) Parallel-connected system. (b) Series-connected system. PS: power supply, TPM: three-phase module.

in Fig. 19(a) and (b), respectively. As a special case, a terminal conversion of isolation transformer is introduced, as shown in Fig. 19(c).

In the three-phase emulating system, the parallel-connected emulating modules are connected without additional terminal conversion parts, as shown in Fig. 20(a). Differently, the series-connected emulating modules in three-phase system need to be connected through additional terminal conversion parts, which can be in the form of transformers or coupling inductors [76], [91], as shown in Fig. 20(b). In [63], the inverter stage consists of several H-bridges in parallel. Two series-connected converters are adopted in [91], where one converter is designed to generate the fundamental voltage and the other is designed to generate the harmonics voltage. In this case, two converters are series-connected through a transformer. A similar circuit is proposed in [76], where the difference lies in the terminal connection components. Three coupling inductors are adopted in this solution.

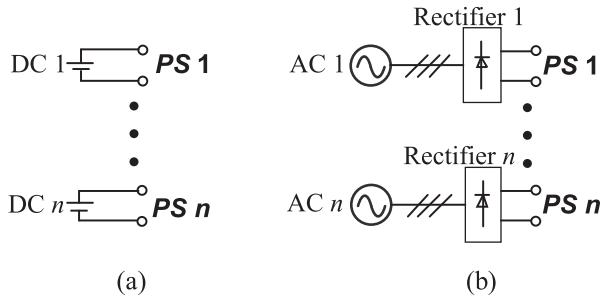

Fig. 21. Individual power supply (a) based on dc power, (b) based on ac power. PS: power supply.

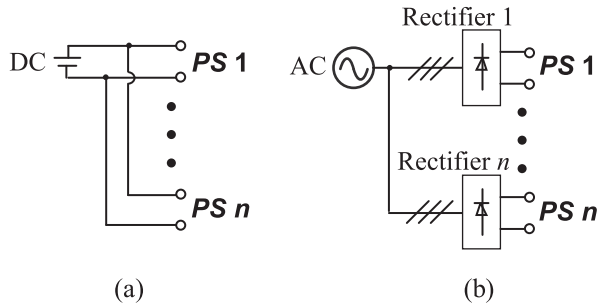

Fig. 22. Common power supply (a) based on dc power, (b) based on ac power. PS: power supply.

B. Power Supply

The optimal power supply solutions for various emulating modules in the grid emulator can be an interesting research topic. As shown in Fig. 21, each emulating converter or power amplifier is powered by individual power source. There is no zero-sequence current issue in this case, while the cost of such system is relatively large, and the power flow in this configuration is hard to be circulated, and the capacity of the power sources needs to be at the similar level of the emulating system.

As shown in Fig. 22, a common power supply solution is indicated, which can be a dc power source [117] or an ac power source [118]. In this solution, the power supplies are connected to dc power sources directly, or are connected to ac power sources through rectifiers. Considering the number of ac/dc power sources, the common power supply is much easier to be achieved. More importantly, the power flow in the emulating modules can be circulated to save the required capacity of the sources, which only need to provide losses in the emulating system. But there are zero-sequence circuit among different power sources, thus, there may be undesired circulating current flowing in power sources.

There are two approaches to eliminate the circulating current, i.e., active approaches [119]–[121] and passive approaches [117], [118]. The active approach is achieved through adding an extra control loop [119] or using an enhanced modulation

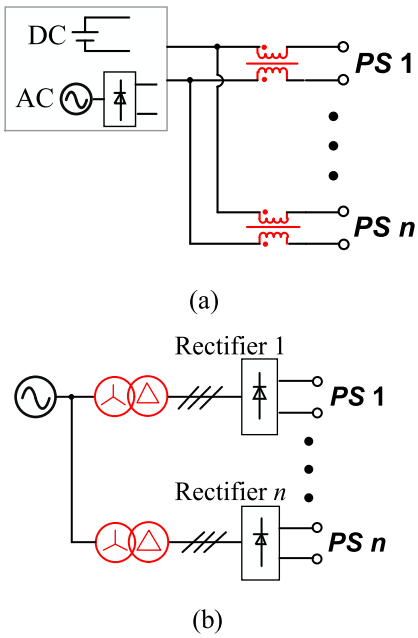

Fig. 23. Zero-sequence current suppression (a) based on common-mode inductors, (b) based on transformers. PS: power supply.

method [120], [121]. The passive approaches are achieved through hardware circuit design, and include mainly two approaches. As shown in Fig. 23(a), the first passive approach is realized by placing a common-mode inductor at the front of each power supply, and the common-mode inductor is designed to eliminate the zero-sequence circulating current [117]. The second passive approach is shown in Fig. 23(b), where a transformer is placed between the ac power source and rectifiers [118]. The primary side of transformer is connected to ac power source and the secondary side is connected to rectifiers. To eliminate the zero-sequence circulating current, the secondary sides of all transformers adopt corner connection method [118]. The first passive approach is hard to achieve because the common-mode inductor is hard to design, compared with the second passive approach. Nevertheless, because the transformers are only available in ac system, the second passive approach must be powered by ac power sources.

VIII. Conclusion

With the increasing penetration of power electronics converters in the power grid, the grid characteristics are altered and sometimes can be complicated. As a result, multiple spatial-scales and timescales of grid emulation is becoming essential. The advanced grid emulation needs to be able to reflect the complex spatial-configuration of grid components with various bandwidth or dynamics. Up until now, four concepts of grid emulation have been reported. However, there are still some technical uncertainties need to be solved.

First, the stability is an important issue in modern power grid, and the existing emulation methods are not capable of emulating the resonance behaviors precisely under different frequency ranges. For example, the concept III is not able to emulate the grid characteristics at high frequency band, and the concept II shrinks the stability region because of the transmission delays caused by the introduced RTS.

Second, the grid code is becoming more complex and requires the grid-connected converters to cooperate with each other. The existing emulation methods mainly focus on the manipulation of the voltage behaviors and more aspects of the dynamics need to be emulated and more CUTs are needed to be tested and communicated simultaneously.

Third, the cost and efficiencies of grid emulator are important issues. The existing concepts of grid emulation are uncapable of emulating complex grid with low cost. The concept III and concept IV are hard to emulate the grid with complex spatial configuration, and the concept II is expensive to achieve at higher power level. The emulation of grid with complex spatial configuration at low cost is an emerging need for the testing of grid-connected converters.

To emulate the grid precisely, the grid with different spatial structure under different frequency ranges need to be clarified and designed. The comparison among four concepts is shown in Table I and a classification based on these two criteria is proposed is shown in Fig. 4 with relevant literatures allocated. The physical components with their controllers make the concept I represent nearly same characteristics with the emulated grid. Therefore, the concept I is usually used for dynamic simulation in conventional power system and stability test for grid-connected converters. The concept II has advantages to emulate the grid with different spatial structures since the grid is modeled in RTS. The connection among different converters in concept III make the interaction between different CUTs is easy to achieve in concept III. The flexibility of control method in concept IV makes the grid characteristics under different frequency ranges easy to be emulated. The circuit configurations of converters or linear circuit used in three concepts and power amplifier is hierarchically classified. The power supply is mainly about the zero-sequence current and the approach to eliminate or emulate zero sequence current.

References

[1] S. Kouro, J. I. Leon, D. Vinnikov, and L. G. Franquelo, "Grid-connected photovoltaic systems: An overview of recent research and emerging PV converter technology," *IEEE Ind. Electron. Mag.*, vol. 9, no. 1, pp. 47–61, Mar. 2015.

[2] F. Blaabjerg and K. Ma, "Future on power electronics for wind turbine systems," *IEEE J. Emerg. Sel. Topics Power Electron.*, vol. 1, no. 3, pp. 139–152, Sep. 2013.

[3] F. Blaabjerg, R. Teodorescu, M. Liserre, and A. V. Timbus, "Overview of control and grid synchronization for distributed power generation systems," *IEEE Trans. Ind. Electron.*, vol. 53, no. 5, pp. 1398–1409, Oct. 2006.

[4] H. Han, X. Hou, J. Yang, J. Wu, M. Su, and J. M. Guerrero, "Review of power sharing control strategies for islanding operation of AC microgrids," *IEEE Trans. Smart Grid.*, vol. 7, no. 1, pp. 200–215, Jan. 2016.

[5] J. C. Vasquez, R. A. Mastromauro, J. M. Guerrero, and M. Liserre, "Voltage support provided by a droop-controlled multifunctional inverter," *IEEE Trans. Ind. Electron.*, vol. 56, no. 11, pp. 4510–4519, Nov. 2009.

[6] D. Pan, X. Wang, F. Liu, and R. Shi, "Transient stability of voltage-source converters with grid-forming control: A design-oriented study," *IEEE J. Emerg. Sel. Topics Power Electron.*, vol. 8, no. 2, pp. 1019–1033, Jun. 2020.

[7] Q. Zhong and G. Weiss, "Synchronverters: Inverters that mimic synchronous generators," *IEEE Trans. Ind. Electron.*, vol. 58, no. 4, pp. 1259–1267, Apr. 2011.

[8] W. Wu *et al.*, "A virtual inertia control strategy for DC microgrids analogized with virtual synchronous machines," *IEEE Trans. Ind. Electron.*, vol. 64, no. 7, pp. 6005–6016, Jul. 2017.

[9] J. Fang, P. Lin, H. Li, Y. Yang, and Y. Tang, "An improved virtual inertia control for three-phase voltage source converters connected to a weak grid," *IEEE Trans. Power Electron.*, vol. 34, no. 9, pp. 8660–8670, Sep. 2019.

[10] Y. Hirase, K. Sugimoto, K. Sakimoto, and T. Ise, "Analysis of Resonance in microgrids and effects of system frequency stabilization using a virtual synchronous generator," *IEEE J. Emerg. Sel. Topics Power Electron.*, vol. 4, no. 4, pp. 1287–1298, Dec. 2016.

[11] X. Wang, F. Blaabjerg, M. Liserre, Z. Chen, J. He, and Y. Li, "An active damper for stabilizing power-electronics-based AC systems," *IEEE Trans. Power Electron.*, vol. 29, no. 7, pp. 3318–3329, Jul. 2014.

[12] L. Jia, X. Ruan, W. Zhao, Z. Lin, and X. Wang, "An adaptive active damper for improving the stability of grid-connected inverters under weak grid," *IEEE Trans. Power Electron.*, vol. 33, no. 11, pp. 9561–9574, Nov. 2018.

[13] H. M. P. and M. T. Bina, "A transformerless medium-voltage STATCOM topology based on extended modular multilevel converters," *IEEE Trans. Power Electron.*, vol. 26, no. 5, pp. 1534–1545, May 2011.

[14] M. Hagiwara, R. Maeda, and H. Akagi, "Negative-sequence reactive-power control by a PWM STATCOM based on a modular multilevel cascade converter (MMCC-SDBC)," *IEEE Trans. Ind. Appl.*, vol. 48, no. 2, pp. 720–729, Mar./Apr. 2012.

[15] M. R. Nasiri, S. Farhangi, and J. Rodríguez, "Model predictive control of a multilevel CHB STATCOM in wind farm application using diophantine equations," *IEEE Trans. Ind. Electron.*, vol. 66, no. 2, pp. 1213–1223, Feb. 2019.

[16] Y. Tang, P. C. Loh, P. Wang, F. H. Choo, F. Gao, and F. Blaabjerg, "Generalized design of high performance shunt active power filter with output LCL filter," *IEEE Trans. Ind. Electron.*, vol. 59, no. 3, pp. 1443–1452, Mar. 2012.

[17] W. U. K. Tareen and S. Mekhielf, "Three-phase transformerless shunt active power filter with reduced switch count for harmonic compensation in grid-connected applications," *IEEE Trans. Power Electron.*, vol. 33, no. 6, pp. 4868–4881, Jun. 2018.

[18] G. Liu, J. Hu, G. Tian, L. Xu, and S. Wang, "Study on high voltage ride through control strategy of PMSG-based wind turbine generation system with SCESU," *J. Eng.*, vol. 2019, no. 17, pp. 4257–4260, Jun. 2019.

[19] A. Calle-Prado, S. Alepuz, J. Bordonau, J. Nicolas-Apruzzese, P. Cortés, and J. Rodriguez, "Model predictive current control of grid-connected neutral-point-clamped converters to meet low-voltage ride-through requirements," *IEEE Trans. Ind. Electron.*, vol. 62, no. 3, pp. 1503–1514, Mar. 2015.

[20] J. M. Guerrero, M. Chandorkar, T. Lee, and P. C. Loh, "Advanced control architectures for intelligent microgrids—Part I: Decentralized and hierarchical control," *IEEE Trans. Power Electron.*, vol. 60, no. 4, pp. 1254–1262, Apr. 2013.

[21] J. M. Guerrero, J. C. Vasquez, J. Matas, L. G. de Vicuna, and M. Castilla, "Hierarchical control of droop-controlled AC and DC microgrids—A general approach toward standardization," *IEEE Trans. Ind. Electron.*, vol. 58, no. 1, pp. 158–172, Jan. 2011.

[22] M. Cespedes and J. Sun, "Impedance modeling and analysis of grid-connected voltage-source converters," *IEEE Trans. Power Electron.*, vol. 29, no. 3, pp. 1254–1261, Mar. 2014.

[23] B. Wen, R. Burgos, D. Boroyevich, P. Mattavelli, and Z. Shen, "AC stability analysis and dq frame impedance specifications in power-electronics-based distributed power systems," *IEEE J. Emerg. Sel. Topics Power Electron.*, vol. 5, no. 4, pp. 1455–1465, Dec. 2017.

[24] X. Wang and F. Blaabjerg, "Harmonic stability in power electronic-based power systems: Concept, modeling, and analysis," *IEEE Trans. Smart Grid.*, vol. 10, no. 3, pp. 2858–2870, May 2019.

[25] IEEE Standard for Interconnection and Interoperability of Distributed Energy Resources With Associated Electric Power Systems Interfaces, IEEE Standard 1547-2018, Apr. 2018, pp. 1–138.

[26] G. Ding, F. Gao, H. Tian, C. Ma, M. Chen, G. He, and Y. Liu, "Adaptive DC-link voltage control of two-stage photovoltaic inverter during low voltage ride-through operation," *IEEE Trans. Power Electron.*, vol. 31, no. 6, pp. 4182–4194, Jun. 2016.

[27] I. J. Balaguer, Q. Lei, S. Yang, U. Supatti, and F. Z. Peng, "Control for grid-connected and intentional islanding operations of distributed power generation," *IEEE Trans. Ind. Electron.*, vol. 58, no. 1, pp. 147–157, Jan. 2011.

[28] P. K. Ray, N. Kishor, and S. R. Mohanty, "Islanding and power quality disturbance detection in grid-connected hybrid power system using wavelet and *S*-transform," *IEEE Trans. Smart Grid.*, vol. 3, no. 3, pp. 1082–1094, Sep. 2012.

[29] K. Ma, U. Choi, and F. Blaabjerg, "Prediction and Validation of wear-out reliability metrics for power semiconductor devices with mission profiles in motor drive application," *IEEE Trans. Power Electron.*, vol. 33, no. 11, pp. 9843–9853, Nov. 2018.

[30] Y. Zhu, K. Ma, and X. Cai, "Thermal characterization method of power semiconductors based on H-bridge testing circuit," *IEEE Trans. Power Electron.*, vol. 34, no. 9, pp. 8268–8273, Sep. 2019.

[31] D. Zhou, H. Wang, and F. Blaabjerg, "Mission profile based system-level reliability analysis of DC/DC converters for a backup power application," *IEEE Trans. Power Electron.*, vol. 33, no. 9, pp. 8030–8039, Sep. 2018.

[32] A. S. Vijay, S. Doolla, and M. C. Chandorkar, "Real-time testing approaches for microgrids," *IEEE J. Emerg. Sel. Topics Power Electron.*, vol. 5, no. 3, pp. 1356–1376, Sep. 2017.

[33] D. Wu, G. Li, M. Javadi, A. M. Malyscheff, M. Hong, and J. N. Jiang, "Assessing impact of renewable energy integration on system strength using site-dependent short circuit ratio," *IEEE Trans. Sustain. Energy*, vol. 9, no. 3, pp. 1072–1080, Jul. 2018.

[34] T. Dragičević, X. Lu, J. C. Vasquez, and J. M. Guerrero, "DC microgrids—Part I: A review of control strategies and stabilization techniques," *IEEE Trans. Power Electron.*, vol. 31, no. 7, pp. 4876–4891, Jul. 2016.

[35] V. Nasirian, S. Moayedi, A. Davoudi, and F. L. Lewis, "Distributed cooperative control of DC microgrids," *IEEE Trans. Power Electron.*, vol. 30, no. 4, pp. 2288–2303, Apr. 2015.

[36] N. Flourentzou, V. G. Agelidis, and G. D. Demetriades, "VSC-based HVDC power transmission systems: An overview," *IEEE Trans. Power Electron.*, vol. 24, no. 3, pp. 592–602, Mar. 2009.

[37] A. Nami, J. Liang, F. Dijkhuizen, and G. D. Demetriades, "Modular multilevel converters for HVDC applications: Review on converter cells and functionalities," *IEEE Trans. Power Electron.*, vol. 30, no. 1, pp. 18–36, Jan. 2015.

[38] Z. Zou, K. Zhou, Z. Wang, and M. Cheng, "Fractional-order repetitive control of programmable AC power sources," *IET Power Electron.*, vol. 7, no. 2, pp. 431–438, Feb. 2014.

[39] T. Liu, D. Wang, and K. Zhou, "High-performance grid simulator using parallel structure fractional repetitive control," *IEEE Trans. Power Electron.*, vol. 31, no. 3, pp. 2669–2679, Mar. 2016.

[40] C. Yin *et al.*, "Design and implementation of a grid-fault emulating power supply based on hardware-in-the-loop simulation," in *Proc. 2nd Int. Future Energy Electron. Conf.*, 2015, pp. 1–6.

[41] O. S. Senturk and A. M. Hava, "A simple sag generator using SSRs," *IEEE Trans. Ind. Appl.*, vol. 48, no. 1, pp. 172–180, Jan./Feb. 2012.

[42] J. Fang, H. Li, Y. Tang, and F. Blaabjerg, "On the inertia of future more-electronics power systems," *IEEE J. Emerg. Sel. Topics Power Electron.*, vol. 7, no. 4, pp. 2130–2146, Dec. 2019.

[43] J. Rocabert, A. Luna, F. Blaabjerg, and P. Rodríguez, "Control of power converters in AC microgrids," *IEEE Trans. Power Electron.*, vol. 27, no. 11, pp. 4734–4749, Nov. 2012.

[44] M. Popat, B. Wu, F. Liu, and N. Zargari, "Coordinated control of cascaded current-source converter based offshore wind farm," *IEEE Trans. Sustain. Energy*, vol. 3, no. 3, pp. 557–565, Jul. 2012.

[45] X. Zeng, J. Yao, Z. Chen, W. Hu, Z. Chen, and T. Zhou, "Co-ordinated control strategy for hybrid wind farms with PMSG and FSIG under unbalanced grid voltage condition," *IEEE Trans. Sustain. Energy*, vol. 7, no. 3, pp. 1100–1110, Jul. 2016.

[46] F. M. Albatsh, S. Mekhilef, S. Ahmad, and H. Mokhlis, "Fuzzy-logic-based UPFC and laboratory prototype validation for dynamic power flow control in transmission lines," *IEEE Trans. Ind. Electron.*, vol. 64, no. 12, pp. 9538–9548, Dec. 2017.

[47] W. Dong, H. Xin, D. Wu, and L. Huang, "Small signal stability analysis of multi-infeed power electronic systems based on grid strength assessment," *IEEE Trans. Power Syst.*, vol. 34, no. 2, pp. 1393–1403, Mar. 2019.

[48] P. Wang, H. Zhou, B. Chen, C. Tian, B. Chen, and B. Sun, "Fault location method in resonant grounded networks based on distributed modulation and compensation adjustment," *IEEE Trans. Power Del.*, vol. 34, no. 5, pp. 1938–1947, Oct. 2019.

[49] D. Dong, B. Wen, D. Boroyevich, P. Mattavelli, and Y. Xue, "Analysis of phase-locked loop low-frequency stability in three-phase grid-connected power converters considering impedance interactions," *IEEE Trans. Ind. Electron.*, vol. 62, no. 1, pp. 310–321, Jan. 2015.

[50] X. Zhang, D. Xia, Z. Fu, G. Wang, and D. Xu, "An improved feedforward control method considering PLL dynamics to improve weak grid stability of grid-connected inverters," *IEEE Trans. Ind. Appl.*, vol. 54, no. 5, pp. 5143–5151, Sep./Oct. 2018.

[51] Z. Li *et al.*, "Research on dynamic simulation of the resonance fault current limiter," in *Proc. Int. Conf. Power Syst. Technol.*, Oct. 2010, pp. 1–6.

[52] W.-N. Chang and C.-J. Wu, "Developing static reactive power compensators in a power system simulator for power education," *IEEE Trans. Power Syst.*, vol. 10, no. 4, pp. 1734–1741, Nov. 1995.

[53] D. Shao, X. Yin, Z. Zhang, W. Chen, and D. Chen, "Experiment research on differential protection for UHV transformer in China," in *Proc. IEEE Power Energy Soc. Gen eral Meeting*, Pittsburgh, PA, USA, Jul. 20–24, 2008, pp. 1–5.

[54] M. Karabacak, L. M. Fernández-Ramírez, T. Kamal, and S. Kamal, "A new hill climbing maximum power tracking control for wind turbines with inertial effect compensation," *IEEE Trans. Ind. Electron.*, vol. 66, no. 11, pp. 8545–8556, Nov. 2019.

[55] A. Hoke, S. Chakraborty, and T. Basso, "A power hardware-in-the-loop framework for advanced grid-interactive inverter testing," in *Proc. IEEE Innov. Smart Grid Technol. Conf.*, 2015, pp. 1–5.

[56] A. Schmitt, M. Gommeringer, J. Kolb, and M. Braun, "A high current, high frequency modular multiphase multilevel converter for power hardware-in-the-loop emulation," in *Proc. Int. Exhib. Conf. Power Electron., Intell. Motion, Renewable Energy Energy Manage.*, 2014, pp. 1–8.

[57] H. Alenius, T. Messo, T. Reinikka, and T. Roinila, "Aggregated modeling and power hardware-in-the-loop emulation of grid impedance," in *Proc. IEEE Energy Convers. Congr. Expo.*, 2018, pp. 4179–4186.

[58] K. Luo, W. Shi, and H. Tang, "Implementation and value of power hardware in the loop testing bed for wind turbines integrated into grid," *J. Eng.*, vol. 2017, no. 13, pp. 1635–1639, 2017.

[59] A. J. Roscoe, A. Mackay, G. M. Burt, and J. R. McDonald, "Architecture of a network-in-the-loop environment for characterizing AC power-system behavior," *IEEE Trans. Ind. Electron.*, vol. 57, no. 4, pp. 1245–1253, Apr. 2010.

[60] K. Mentesidi, E. Rikos, V. Kleftakis, P. Kotsampopoulos, M. Santamaria, and M. Aguado, "Implementation of a microgrid model for DER integration in real-time simulation platform," in *Proc. IEEE 23rd Int. Symp. Ind. Electron.*, 2014, pp. 2274–2279.

[61] P. C. Kotsampopoulos, V. A. Kleftakis, and N. D. Hatziargyriou, "Laboratory education of modern power systems using PHIL simulation," *IEEE Trans. Power Syst.*, vol. 32, no. 5, pp. 3992–4001, Sep. 2017.

[62] T. Roinila *et al.*, "Hardware-in-the-loop methods for real-time frequency-response measurements of on-board power distribution systems," *IEEE Trans. Ind. Electron.*, vol. 66, no. 7, pp. 5769–5777, Jul. 2019.

[63] C. Mao *et al.*, "A 400-V/50-kVA digital–physical hybrid real-time simulation platform for power systems," *IEEE Trans. Ind. Electron.*, vol. 65, no. 5, pp. 3666–3676, May 2018.

[64] R. Ferrer-San-José, E. Prieto-Araujo, and O. Gomis-Bellmunt, "Implementation of a power hardware in the loop platform with a real time power flow calculation using PSS\E," in *Proc. Eur. Conf. Power Electron.*, 2017, pp. P.1–P.8.

[65] P. Kotsampopoulos, D. Lagos, N. Hatziargyriou, M. O. Faruque, G. Lauss, O. Nzimako, P. Forsyth, M. Steurer, F. Ponci, A. Monti, V. Dinavahi, and K. Strunz, "A benchmark system for hardware-in-the-loop testing of distributed energy resources," *IEEE Power Energy Technol. Syst. J.*, vol. 5, no. 3, pp. 94–103, Sep. 2018.

[66] F. Guo *et al.*, "Design and development of a reconfigurable hybrid microgrid testbed," in *Proc. IEEE Energy Convers. Congr. Expo.*, 2013, pp. 1350–1356.

[67] B. Palmintier, B. Lundstrom, S. Chakraborty, T. Williams, K. Schneider, and D. Chassin, "A power hardware-in-the-loop platform with remote distribution circuit cosimulation," *IEEE Trans. Ind. Electron.*, vol. 62, no. 4, pp. 2236–2245, Apr. 2015.

[68] J. Wang, Y. Song, W. Li, J. Guo, and A. Monti, "Development of a universal platform for hardware in-the-loop testing of microgrids," *IEEE Trans. Ind. Inform.*, vol. 10, no. 4, pp. 2154–2165, Nov. 2014.

[69] G. De Carne, G. Buticchi, T. Kerekes, and M. Liserre, "Power-hardware-in-loop harmonic analysis of a smart transformer-fed distribution grid," in *Proc. 42nd Annu. Conf. IEEE Ind. Electron. Soc.*, 2016, pp. 7004–7009.

[70] G. F. Lauss, M. O. Faruque, K. Schoder, C. Dufour, A. Viehweider, and J. Langston, "Characteristics and design of power hardware-in-the-loop simulations for electrical power systems," *IEEE Trans. Ind. Electron.*, vol. 63, no. 1, pp. 406–417, Jan. 2016.

[71] M. Maniatopoulos, D. Lagos, P. Kotsampopoulos, and N. Hatziargyriou, "Combined control and power hardware in-the-loop simulation for testing smart grid control algorithms," *IET Gener., Transmiss. Distrib.*, vol. 11, no. 12, pp. 3009–3018, Aug. 24, 2017.

[72] A. F. Hoke, A. Nelson, S. Chakraborty, F. Bell, and M. McCarty, "An islanding detection test platform for multi-inverter islands using power HIL," *IEEE Trans. Ind. Electron.*, vol. 65, no. 10, pp. 7944–7953, Oct. 2018.

[73] S. Amamra, F. Colas, X. Guillaud, P. Rault, and S. Nguefeu, "Laboratory demonstration of a multiterminal VSC-HVDC power grid," *IEEE Trans. Power Del.*, vol. 32, no. 5, pp. 2339–2349, Oct. 2017.

[74] M. Pape, M. A. Allam, and M. Kazerani, "Design and implementation of a highly reconfigurable microgrid test bed platform," in *Proc. IEEE Can. Conf. Elect. Comput. Eng.*, 2016, pp. 1–6.

[75] J. Montano, C. Leon, A. Garcia, A. Lopez, I. Monedero, and E. Personal, "Random generation of arbitrary waveforms for emulating three-phase systems," *IEEE Trans. Ind. Electron.*, vol. 59, no. 11, pp. 4032–4040, Nov. 2012.

[76] G. Si, J. Cordier, and R. M. Kennel, "Extending the power capability with dynamic performance of a power-hardware-in-the-loop application—Power grid emulator using "inverter cumulation"," *IEEE Trans. Ind. Appl.*, vol. 52, no. 4, pp. 3193–3202, Jul./Aug. 2016.

[77] F. Wang, L. Zhang, X. Feng, and H. Guo, "An adaptive control strategy for virtual synchronous generator," *IEEE Trans. Ind. Appl.*, vol. 54, no. 5, pp. 5124–5133, Sep./Oct. 2018.

[78] M. Guan, W. Pan, J. Zhang, Q. Hao, J. Cheng, and X. Zheng, "Synchronous generator emulation control strategy for voltage source converter (VSC) stations," *IEEE Trans. Power Syst.*, vol. 30, no. 6, pp. 3093–3101, Nov. 2015.

[79] L. Zhu, D. Jiang, and R. Qu, "Power converter-based aircraft starting/generating system emulator," in *Proc. 43rd Annu. Conf. IEEE Ind. Electron. Soc.*, 2017, pp. 4165–4170.

[80] Y. Ma, L. Yang, F. Wang, and L. M. Tolbert, "Short circuit fault emulation by shunt connected voltage source converter," in *Proc. IEEE Energy Convers. Congr. Expo.*, 2015, pp. 2622–2628.

[81] J. Liu, Y. Miura, and T. Ise, "Comparison of dynamic characteristics between virtual synchronous generator and droop control in inverter-based distributed generators," *IEEE Trans. Power Electron.*, vol. 31, no. 5, pp. 3600–3611, May 2016.

[82] S. Li, W. Qi, S. Tan, S. Y. Hui, and C. K. Tse, "A general approach to programmable and reconfigurable emulation of power impedances," *IEEE Trans. Power Electron.*, vol. 33, no. 1, pp. 259–271, Jan. 2018.

[83] G. Karthick, C. Gokul, A. Vijayakumari, P. Sujith, A. Suyampulingam, and N. P. Kumar, "Design and implementation of a fault emulator for LVRT capability testing of wind turbines," in *Proc. Int. Elect. Electron. Eng. Commun. Optim. Sci.*, 2016, pp. 1–5.

[84] H. Akbarian, P. Pillay, and L. Lopes, "Design of a power electronic emulator for parallel operation of renewable energy resources in microgrids," in *Proc. IEEE Int. Elect. Mach. Drives Conf.*, 2015, pp. 1532–1537.

[85] H. Wu *et al.*, "Small-signal modeling and parameters design for virtual synchronous generators," *IEEE Trans. Ind. Electron.*, vol. 63, no. 7, pp. 4292–4303, Jul. 2016.

[86] S. Zhang, B. Liu, S. Zheng, Y. Ma, F. Wang, and L. M. Tolbert, "Development of a converter-based transmission line emulator with three-phase short-circuit fault emulation capability," *IEEE Trans. Power Electron.* vol. 33, no. 12, pp. 10215–10228, Dec. 2018.

[87] S. Skander-Mustapha, M. J. Ghorbal, M. Miladi, and I. Slama-Belkhodja, "Load analysis effect on grid fault emulator," in *Proc. 9th Int. Renewable Energy Congr.*, 2018, pp. 1–6.

[88] M. Díaz, R. Cárdenas, F. Rojas, and J. Clare, "3-phase 4-wire matrix converter-based voltage sag/swell generator to test low-voltage ride through in wind energy conversion systems," *IET Power Electron.*, vol. 7, no. 12, pp. 3116–3125, Dec. 2014.

[89] N. N. K and L. Umanand, "A virtual impedance based grid emulator for the performance analysis of distributed generations," in *Proc. IEEE Appl. Power Electron. Conf. Expo.*, 2019, pp. 3013–3018.

[90] J. He, Y. W. Li, and F. Blaabjerg, "An enhanced islanding microgrid reactive power, imbalance power, and harmonic power sharing scheme," *IEEE Trans. Power Electron.*, vol. 30, no. 6, pp. 3389–3401, Jun. 2015.

[91] Y. Hu, J. Cheng, Y. Zhou, and G. Chen, "Control strategy of a high power grid simulator for the test of renewable energy grid converter," in *Proc. 43rd Annu. Conf. IEEE Ind. Electron. Soc.*, 2017, pp. 7747–7752.

[92] B. C. Waltrip *et al.*, "AC power standard using a programmable josephson voltage standard," *IEEE Trans. Instrum. Meas.*, vol. 58, no. 4, pp. 1041–1048, Apr. 2009.
[93] S. A. Richter, J. von Bloh, C. P. Dick, D. Hirschmann, and R. W. De Doncker, "Control of a medium-voltage test generator," in *Proc. IEEE P ower E lectron. S pecialists C onf.*, 2008, pp. 3787–3793.
[94] J. Wang *et al.*, "Static and dynamic power system load emulation in converter-based reconfigurable power grid emulator," *IEEE Trans. Power Electron.*, vol. 31, no. 4, pp. 3239–3251, Apr. 2016.
[95] Y. Hu, Y. Shao, R. Yang, X. Long, and G. Chen, "A configurable virtual impedance method for grid-connected virtual synchronous generator to improve the quality of output current," *IEEE J. Emerg. Sel. Topics Power Electron.*, vol. 8, no. 3, pp. 2404–2419, Sep. 2020.
[96] L. Yang *et al.*, "Development of converter based reconfigurable power grid emulator," in *Proc. IEEE Energy Convers. Congr. Expo.*, 2014, pp. 3990–3997.
[97] Y. Li, X. Shi, B. Liu, W. Lei, F. Wang, and L. M. Tolbert, "Development, demonstration, and control of a testbed for multiterminal HVDC system," *IEEE Trans. Power Electron.*, vol. 32, no. 8, pp. 6069–6078, Aug. 2017.
[98] A. S. Vijay, S. Doolla, and M. C. Chandorkar, "A highly reconfigurable system emulator for testing AC microgrids," in *Proc. IEEE Energy Convers. Congr. Expo.*, 2017, pp. 1567–1574.
[99] D. J. Hogan, M. G. Egan, J. G. Hayes, G. Lightbody, and F. Gonzalez-Espin, "A rapid prototyping tool for load and source emulation in a microgrid test laboratory," in *Proc. IEEE Appl. Power Electron. Conf. Expo.*, 2014, pp. 2245–2252.
[100] J. Roldán-Pérez, A. Rodríguez-Cabero, and M. Prodanović, "Harmonic virtual impedance design for parallel-connected grid-tied synchronverters," *IEEE J. Emerg. Sel. Topics Power Electron.*, vol. 7, no. 1, pp. 493–503, Mar. 2019.
[101] H. Tian, Y. W. Li, and P. Wang, "Hybrid AC/DC system harmonics control through grid interfacing converters with low switching frequency," *IEEE Trans. Ind. Electron.*, vol. 65, no. 3, pp. 2256–2267, Mar. 2018.
[102] H. Tian, X. Wen, and Y. W. Li, "A harmonic compensation approach for interlinking voltage source converters in hybrid AC-DC microgrids with low switching frequency," *CSEE J. Power Energy Syst.*, vol. 4, no. 1, pp. 39–48, Mar. 2018.
[103] S. Mukherjee, P. Shamsi, and M. Ferdowsi, "Indirect voltage control of a stand-alone inverter," in *Proc. IEEE Appl. Power Electron. Conf. Expo.*, 2017, pp. 3451–3455.
[104] X. Wang, Y. Pang, P. C. Loh, and F. Blaabjerg, "A series-LC-filtered active damper with grid disturbance rejection for AC power-electronics-based power systems," *IEEE Trans. Power Electron.*, vol. 30, no. 8, pp. 4037–4041, Aug. 2015.
[105] S. Yoon, H. Oh, and S. Choi, "Controller design and implementation of indirect current control based utility-interactive inverter system," *IEEE Trans. Power Electron.*, vol. 28, no. 1, pp. 26–30, Jan. 2013.
[106] W. Ren, M. Steurer, and T. L. Baldwin, "Improve the stability and the accuracy of power hardware-in-the-loop simulation by selecting appropriate interface algorithms," *IEEE Trans. Ind. Appl.*, vol. 44, no. 4, pp. 1286–1294, Jul./Aug. 2008.
[107] G. Gong, D. Hassler, and J. W. Kolar, "A comparative study of multi-cell amplifiers for AC-power-source applications," *IEEE Trans. Power Electron.*, vol. 26, no. 1, pp. 149–164, Jan. 2011.
[108] A. Sanchez, A. de Castro, and J. Garrido, "A comparison of simulation and hardware-in-the-loop alternatives for digital control of power converters," *IEEE Trans. Ind. Inform.*, vol. 8, no. 3, pp. 491–500, Aug. 2012.
[109] S. Jeng and Y. Tung, "A multicell linear power amplifier for driving piezoelectric loads," *IEEE Trans. Ind. Electron.*, vol. 55, no. 10, pp. 3644–3652, Oct. 2008.
[110] J. He, L. Du, B. Liang, Y. Li, and C. Wang, "A coupled virtual impedance for parallel AC/DC converter based power electronics system," *IEEE Trans. Smart Grid*, vol. 10, no. 3, pp. 3387–3400, May 2019.
[111] X. Li, Z. Deng, Z. Chen, and Q. Fei, "Analysis and simplification of three-dimensional space vector PWM for three-phase four-leg inverters," *IEEE Trans. Ind. Electron.*, vol. 58, no. 2, pp. 450–464, Feb. 2011.
[112] S. Chee, S. Ko, H. Kim, and S. Sul, "Common-mode voltage reduction of three-level four-leg PWM converter," *IEEE Trans. Ind. Appl.*, vol. 51, no. 5, pp. 4006–4016, Sep./Oct. 2015.
[113] J. A. Valle-Mayorga, A. Rahman, and H. A. Mantooth, "A SiC NMOS linear voltage regulator for high-temperature applications," *IEEE Trans. Power Electron.*, vol. 29, no. 5, pp. 2321–2328, May 2014.
[114] G. Gong, H. Ertl, and J. W. Kolar, "Novel tracking power supply for linear power amplifiers," *IEEE Trans. Ind. Electron.*, vol. 55, no. 2, pp. 684–698, Feb. 2008.
[115] P. Koralewicz, V. Gevorgian, R. Wallen, W. van der Merwe, and P. Jörg, "Advanced grid simulator for multi-megawatt power converter testing and certification," in *Proc. IEEE Energy Convers. Congr. Expo.*, 2016, pp. 1–8.
[116] G. S. da Silva, R. C. Beltrame, L. Schuch, and C. Rech, "Hybrid AC power source based on modular multilevel converter and linear amplifier," *IEEE Trans. Power Electron.*, vol. 30, no. 1, pp. 216–226, Jan. 2015.
[117] K. Saito and H. Akagi, "A power hardware-in-the-loop (P-HIL) test bench using two modular multilevel DSCC converters for a synchronous motor drive," *IEEE Trans. Ind. Appl.*, vol. 54, no. 5, pp. 4563–4573, Sep./Oct. 2018.
[118] J. Shen *et al.*, "A high-frequency high-power test bench for 11 MW/595 Hz drives with 1.25 MW grid capability," *IEEE Trans. Ind. Appl.*, vol. 53, no. 5, pp. 4744–4756, Sep./Oct. 2017.
[119] F. Wang, Y. Wang, Q. Gao, C. Wang, and Y. Liu, "A control strategy for suppressing circulating currents in parallel-connected PMSM drives with individual DC links," *IEEE Trans. Power Electron.*, vol. 31, no. 2, pp. 1680–1691, Feb. 2016.
[120] J. Wang, F. Hu, W. Jiang, W. Wang, and Y. Gao, "Investigation of zero sequence circulating current suppression for parallel three-phase grid-connected converters without communication," *IEEE Trans. Ind. Electron.*, vol. 65, no. 10, pp. 7620–7629, Oct. 2018.
[121] M. H. Ravanji, N. Amouzegar Ashtiani, M. Parniani, and H. Mokhtari, "Modeling and control of zero-sequence circulating current in parallel converters with space vector modulation," *IEEE J. Emerg. Sel. Topics Power Electron.*, vol. 5, no. 1, pp. 363–377, Mar. 2017.
[122] A. Myaing and V. Dinavahi, "FPGA-based real-time emulation of power electronic systems with detailed representation of device characteristics," *IEEE Trans. Ind. Electron.*, vol. 58, no. 1, pp. 358–368, Jan. 2011.
[123] Gu. Si and R. Kennel, "Comparative study of PI controller and quadratic optimal regulator applied for a converter based PHIL grid emulator," in *Proc. IEEE 8th Int. Power Electron. Motion Control Conf.*, 2016, pp. 768–775.

Ke Ma (Senior Member, IEEE) received the B.Sc. and M.Sc. degrees in electrical engineering from Zhejiang University, Hangzhou, China, in 2007 and 2010, respectively, and the Ph.D. degree from the Aalborg University, Aalborg, Denmark, in 2013.

He was an Assistant Professor with Aalborg University, in 2014. He was a Part-Time Consultant with Vestas Wind Systems A/S, Aarhus, Denmark, in 2015. In 2016, he was with the Faculty of Shanghai Jiao Tong University, Shanghai, China, as a tenure-track Research Professor, and is currently serving as the Deputy Director with the Key Laboratory of Control of Power Transmission and Conversion, Ministry of Education, China. His research interests include the power electronics and its reliability in the application of renewable energy, HVdc, and motor drive systems.

Dr. Ma is currently serving as an Associate Editor for IEEE TRANSACTIONS ON INDUSTRY APPLICATIONS and IEEE JOURNAL OF EMERGING AND SELECTED TOPICS IN POWER ELECTRONICS. In 2016, he was the recipient of the "Thousand Talents Plan Program for Young Professionals" of China. He was the recipient of the "Excellent Young Wind Doctor Award 2014" by European Academy of Wind Energy, and several prized paper awards by IEEE.

Jiashi Wang received the B.Sc. and M.Sc. degrees in electrical engineering from China University of Mining and Technology, Xuzhou, China, in 2015 and 2018, respectively. He is currently working toward the Ph.D. degree with the Department of Electrical Engineering, Shanghai Jiao Tong University, Shanghai, China.

His research interests include control of dc/ac converter and mission profile emulators for grid-connected converters.

Xu Cai received the B.Eng. degree from Southeast University, Nanjing, China, in 1983, and the M.Sc. and Ph.D. degrees from China University of Mining and Technology, Xuzhou, China, in 1988 and 2000, respectively.

He was an Associate Professor with the Department of Electrical Engineering, China University of Mining and Technology, from 1989 to 2001. He was the Vice Director of the State Energy Smart Grid R&D Center, Shanghai, China, from 2010 to 2013. Since 2002, he has been with Shanghai Jiao Tong University, Shanghai, as a Professor, where he has also been the Director of the Wind Power Research Center, since 2008. His research interests include power electronics and renewable energy exploitation and utilization, including wind power converters, wind turbine control system, large power battery storage systems, clustering of wind farms and its control system, and grid integration.

Frede Blaabjerg (Fellow, IEEE) received the Ph.D. degree in electrical engineering from Aalborg University, Aalborg, Denmark, in 1995, and honoris causa degree from University Politehnica Timisoara (UPT), Timisoara, Romania, in 2017, and the honoris causa degree from Tallinn Technical University (TTU), Tallinn, Estonia, in 2018.

He was with ABB-Scandia, Randers, Denmark, from 1987 to 1988. He was an Assistant Professor in 1992, an Associate Professor in 1996, and a Full Professor of power electronics and drives in 1998. From 2017, he became a Villum Investigator. He has authored/coauthored more than 600 journal papers in the fields of power electronics and its applications. He has coauthored four monographs and is an editor of ten books in power electronics and its applications. His research interests include power electronics and its applications such as in wind turbines, PV systems, reliability, harmonics, and adjustable speed drives.

Prof. Blaabjerg was the recipient of 32 IEEE Prize Paper Awards, the IEEE PELS Distinguished Service Award, in 2009, the EPE-PEMC Council Award, in 2010, the IEEE William E. Newell Power Electronics Award 2014, the Villum Kann Rasmussen Research Award 2014, the Global Energy Prize in 2019, and the 2020 IEEE Edison Medal. He was the Editor-in-Chief of the IEEE TRANSACTIONS ON POWER ELECTRONICS from 2006 to 2012. He has been a Distinguished Lecturer for the IEEE Power Electronics Society from 2005 to 2007 and for the IEEE Industry Applications Society from 2010 to 2011 as well as 2017 to 2018. In 2019–2020, he serves as the President of IEEE Power Electronics Society. He is the Vice-President of the Danish Academy of Technical Sciences too. He is nominated in 2014–2019 by Thomson Reuters to be among the 250 most-cited researchers in engineering in the world.